(12)

OFFICE OF NAVAL RESEARCH
Contract N00014-80-C-0798

Final Report
June 1986

STABILITY OF UV OPTICAL COATINGS IN HOSTILE EXCIMER LASER ENVIRONMENTS

M. A. Loudiana and J. Thomas Dickinson

Washington
State University

DEPARTMENT OF PHYSICS

(12)

OFFICE OF NAVAL RESEARCH
Contract N00014-80-C-0798

Final Report
June 1986

STABILITY OF UV OPTICAL COATINGS IN HOSTILE EXCIMER LASER ENVIRONMENTS

M. A. Loudiana and J. Thomas Dickinson

Department of Physics
Washington State University
Pullman, Washington 99164-2814

Approved for public release; distribution unlimited.

Unclassified

SECURITY CLASSIFICATION OF THIS PAGE (When Data Entered)

REPORT DOCUMENTATION PAGE		READ INSTRUCTIONS BEFORE COMPLETING FORM
1 REPORT NUMBER	2. GOVT ACCESSION NO.	3 RECIPIENT'S CATALOG NUMBER
4. TITLE (and Subtitle) Stability of UV Optical Coatings in Hostile Excimer Laser Environments		5 TYPE OF REPORT & PERIOD COVERED Final Report July 1980 - Dec. 1985 6 PERFORMING ORG. REPORT NUMBER
7 AUTHOR(s) M. A. Loudiana and J. T. Dickinson		8. CONTRACT OR GRANT NUMBER(s) N00014-80-C-0798
9 PERFORMING ORGANIZATION NAME AND ADDRESS Department of Physics Washington State University Pullman, WA 99164-2814		10 PROGRAM ELEMENT PROJECT TASK AREA & WORK UNIT NUMBERS
11 CONTROLLING OFFICE NAME AND ADDRESS Office of Naval Research Physics Program 800 N. Quincy St., Arlington, VA 22217		12. REPORT DATE June 15, 1986 13 NUMBER OF PAGES 101
14 MONITORING AGENCY NAME & ADDRESS (if different from Controlling Office)		15 SECURITY CLASS (of this report) Unclassified 15a. DECLASSIFICATION DOWNGRADING SCHEDULE

16 DISTRIBUTION STATEMENT (of this Report)

Approved for public release; distribution unlimited

17 DISTRIBUTION STATEMENT (of the abstract entered in Block 20, if different from Report)

18. SUPPLEMENTARY NOTES

19 KEY WORDS (Continue on reverse side if necessary and identify by block number)

Optical coatings, excimer laser, laser damage, reactive etching, optical thin films, mass spectroscopy, mass loss, surface reactions, oxide films, halide films, XeF_2, F_2, NF_2, tungsten, chemisorption, chemisorptive emission

20 ABSTRACT (Continue on reverse side if necessary and identify by block number)

Experiments simulating the exposure of optical coating materials to excimer laser environments are reported. Included are studies of the effect of ion bombardment on SiO_2 exposed to XeF_2; the effect of electron bombardment on a Ag surface (clean, or under thin films of ThF_4, MgF_2, SiO_2, or Al_2O_3) in the presence of XeF_2 or F_2; the effect of electron bombardment on ThF_4 exposed to XeF_2; and electron emission from F_2 adsorption on tungsten, with a model for the F_2 flux dependence and temperature dependence of this phenomenon.

DD FORM 1 JAN 73 1473 EDITION OF 1 NOV 65 IS OBSOLETE

Unclassified

SECURITY CLASSIFICATION OF THIS PAGE (When Data Entered)

TABLE OF CONTENTS

I. TECHNICAL SUMMARY

The addition of energetic radiation to a gas-solid surface system may initiate or enhance chemical reactions occurring on the surface. Conversely, when a chemical reaction proceeds on a surface, radiation may be spontaneously emitted.

The effect of argon ion bombardment on SiO_2 exposed to XeF_2 was studied. At room temperature SiO_2 adsorbs a monolayer of fluorine when exposed to XeF_2. It was found that the adsorbed fluorine layer is responsible for a 3.5 fold enhancement in the ion sputtering rate in the presence of XeF_2.

The effect of electron bombardment on a silver surface in the presence of XeF_2 and F_2 was studied. It was discovered that a multilayer adsorption of fluorine occurs during exposure of a silver surface to F_2 or XeF_2. As silver fluoride was formed on the surface, XeF_2 adsorbed more rapidly. Under the influence of electron bombardment, the rates of adsorption increased due to the formation of a mobile, reactive fluorine species. This phenomenon was found to occur when thin films of SiO_2, Al_2O_3, ThF_4, or MgF_2 were deposited on the silver.

The effect of electron bombardment on ThF_4 exposed to XeF_2 was studied. During electron bombardment, a ThF_4 film was found to lose the equivalent of all of the

fluorine in 27 monolayers. When the fluorine depleted surface was exposed to XeF_2, it rapidly gained back 1 monolayer of fluorine. When ThF_4 was electron bombarded in the presence of XeF_2, much less fluorine was lost. Under certain conditions, ThF_4 was found to rapidly adsorb multilayers of fluorine.

The emission of electrons from the adsorption of F_2 on tungsten was studied. An emission probability of 10^{-10} was determined. A simple kinetic model was developed which agrees well with the data. The emission rapidly increases with temperature due to the electron population in the tungsten shifting to higher energies, above the Fermi level. Emission was not observed during the adsorption of XeF_2 on tungsten.

II. INTRODUCTION

Understanding how radiation affects chemical reactions occurring on surfaces is important because it enables us to understand how well materials will survive in an environment which contains corrosive gases and energetic radiation. One such environment exists inside an excimer laser, where the optical components are exposed to flucrine containing gases, electrons, ions, and reactive radicals in the presence of an intense photon flux. A breakdown of the optical coating thin films exposed to this environment often renders the entire laser useless.

Knowledge of how radiation affects surface chemical reactions can be useful in manufacturing submicron structures for VLSI (1-4) or integrated optics (optical computer) applications. In typical manufacturing applications the material to be etched is masked with a difficult to etch material (as in Fig. 2.1a). The etchant gas is then directed at the surface. In an isotropic etch radiation is not used and the gas molecules are able to etch the surface in any direction. This results in an abundance of material removed under the mask (undercutting) as in Fig. 2.1b. If a radiation induced reaction is used to etch the surface, etching only occurs on the surfaces illuminated with the radiation. This results in a vertical

DIRECTIONALITY OF ETCHING PROCESS

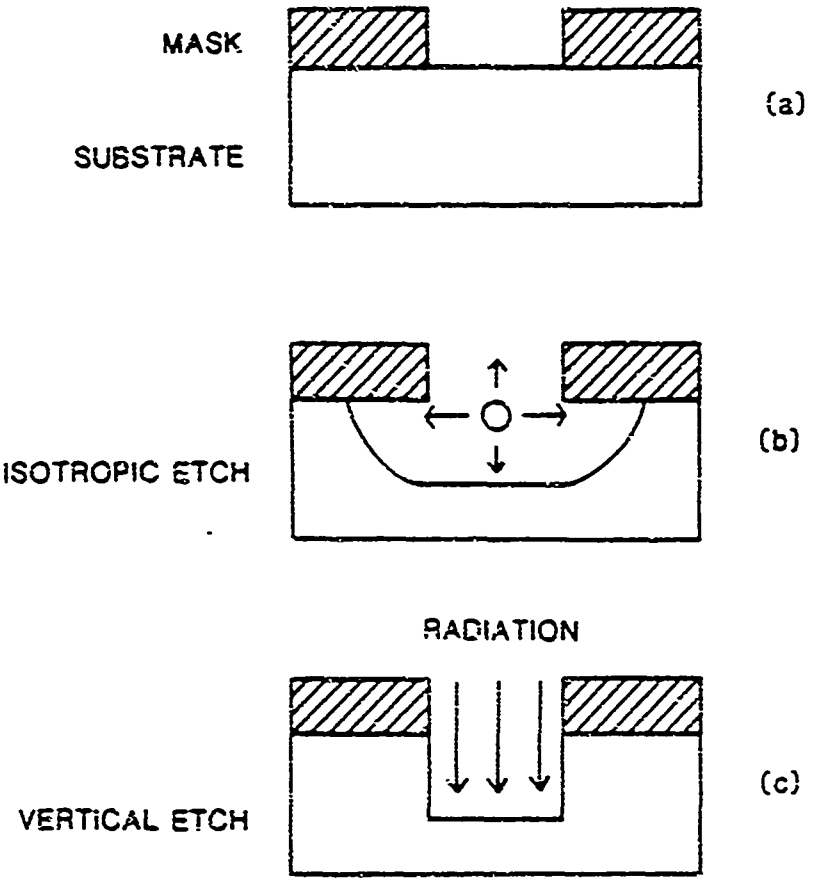

Fig. 2.1 (a) Manufacture of IC's involves etching a pattern in the substrate using a mask. (b) Isotropic etching undercuts the mask. (c) Use of radiation induced etching only etches the surface illuminated by the radiation.

etch profile as illustrated in Fig. 2.1c. Vertical etching allows smaller structures to be etched and larger device densities to be placed on a chip.

CHEMICAL REACTIONS ON SURFACES

When a solid surface comes in contact with a reactive gas, a chemical reaction may take place on the surface. A surface reaction can typically be divided into 3 processes: adsorption, product formation, and product desorption (1-21). The reaction is initiated when molecules from the gas phase chemisorb on the surface. During this adsorption process radiation may be emitted by the surface (22-35). The product formation process may involve the physical rearrangement of atoms on the surface as well as a rearrangement of their electronic structure. The volatile product molecule may then desorb from the surface leaving behind a site for adsorption. If the product molecule fails to desorb, the reaction may not proceed past 1 monolayer.

When radiation (usually in the form of ions, electrons, or photons) is incident on a surface, the rate at which a chemical reaction will proceed can be greatly affected. Radiation can increase the rate of reaction (1-12,15,19,36-45). The presence of radiation may slow or completely stop a surface chemical reaction (1) due to the

production of nonvolatile products. Radiation may also stimulate a reaction to occur in gas-surface systems where no reaction occurs spontaneously (1,4,8,9,15,16,18,19,41,46-58).

REACTIVE ION ETCHING

When a solid surface is bombarded with sufficiently energetic ions, an atomic collision cascade is initiated which can result in the ejection of atoms from the surface (59-64). This process is called ion sputtering. An important variable in ion sputtering is the sputtering yield, which is equal to the number of surface atoms ejected for each incident ion. If the surface contains more than one type of atom, the sputtering yields for each species may be different (60,66-68). This leads to an enrichment in the surface concentration of the species with the lower sputtering yield (65,66).

When the sputtering yield is increased by the addition of a gas, this increase is often called the chemical sputtering yield (8,44,45,55). One can either think of the gas as enhancing the sputtering yield, or the ion bombardment as enhancing the chemical reaction rate on the surface. There are several mechanisms by which ion bombardment can enhance or initiate a chemical reaction between a gas and a solid surface. Ion bombardment tends

to produce a rough and highly defective surface (50,67). This tends to increase the sticking probabilities for various gases (68) and thus enhances the adsorption process (7). Ion bombardment also tends to rearrange the positions of atoms on the surface away from their room temperature equilibrium positions. In addition, some of the energy of the incoming ion is transferred to the electronic structure of the surface as is evidenced by electron emission during ion bombardment (69,70). These two phenomena may enhance the formation of a volatile product (7,19). Ion sputtering also removes nonvolatile products formed with a low binding energy to the surface. This provides fresh surface for the continuation of the reaction and can greatly increase the reaction rate (8).

In Section IV, a study on the chemical sputtering of SiO_2 in the presence of XeF_2 and Ar ions is reported. An adsorbed fluorine layer is found to be responsible for a 3.5 fold enhancement in the sputtering yield of SiO_2 in such an environment. It is concluded that ion bombardment of SiO_2 in XeF_2 enhances product formation or product desorption.

ELECTRON STIMULATED EFFECTS

Electron bombardment of a solid surface can result in a number of processes. If gas molecules are adsorbed o

the surface, electron bombardment can result in the desorption of some of these molecules (electron stimulated desorption: ESD, 17,41,50,71-77). Energetic electrons incident on the surface of a compound often result in the dissociation of the compound near the surface and the desorption of one or more atomic species in the form of ions or neutral particles (78-86). Two models exist to explain these phenomena. One model proposed by Menzel, Gomer, and Redhead (MGR) involves a Franck-Condon excitation caused by electron or photon impact (41,71,72,74,76). If the excitation involves a nonbonding state, the affected particle will begin to move away from the surface. If the excited state is long lived and not quenched by the surface, the particle will desorb.

A second model proposed by Knotek and Feibelman (71,72,74-76,81,82), involves a core hole ionization of one component of an ionic system. This is followed by an Auger de-excitation from a negative anion which results in a positively charged ion. This positive ion is electrostatically repelled by the neighboring positively charged cations from the surface.

In addition to these effects, electron bombardment has been reported to stimulate a number of chemical reactions on a surface in the presence of a gas or adsorbate (17-19,38-40,50). The creation of electronic defects and ESD of an adsorbed layer may enhance the

adsorption process. The energy of an electron incident on a surface is almost completely absorbed by the electronic structure of the solid in the first few atomic layers (68). This energy is available to overcome activation barriers associated with chemical reaction and diffusion, which may aid in product formation. In addition, product desorption may be enhanced by ESD.

In Section VI a study on electron induced damage of ThF_4 films in the presence of XeF_2 is reported. The effects of electron bombardment on a ThF_4 surface was analyzed, as well as the subsequent uptake of fluorine after electron bombardment is halted and the surface is exposed to XeF_2. The effect of simultaneous exposure of ThF_4 to XeF_2 and energetic electrons is reported and the effect of XeF_2 flux, electron flux, and electron energy on this phenomenon is reported.

During the initial studies of the effect of simultaneous electron bombardment and XeF_2 exposure on ThF_4, the silver substrate was found to participate in an electron stimulated reaction. This is the subject of Section V. In Section V the adsorption of fluorine from gaseous F_2 and XeF_2 on silver was investigated along with the electron stimulated formation of silver fluoride. This phenomenon was found to occur even when thin film barriers existed on the silver surface.

CHEMISORPTIVE EMISSION AND CHEMILUMINESCENCE

Emission of radiation during a surface chemical reaction usually occurs during the adsorption phase (22-35). However, the desorption of excited particles which radiate in the gas phase has also been reported (87). In the model of Norskov and Kasemo (30,33,34) emission during adsorption is due to the de-excitation of an excited state present on the surface during the adsorption process. This excited state is formed nonadiabatically by the rapid approach of the molecule toward the surface. The excited state is in the form of an electron hole in the adsorbate electronic structure below the Fermi level of the solid. The level is filled by a radiative or non-radiative (Auger) process from electrons in the solid (30,33,34). This emission is detected as chemisorptive emission (CE) and chemiluminescence (CL).

In Section VII CE from the exposure of polycrystalline tungsten to gaseous F_2 and XeF_2 is examined. Metal-halogen interactions are of considerable interest to metalization processes and reactive etching of metals in thin films and VLSI technologies. A simple kinetic model is applied to CE from the exposure of tungsten to F_2. The apparent lack of CE from the exposure of tungsten to XeF_2 is explained in terms of the large molecular mass of XeF_2 which results in a vanishingly small

probability for the nonadiabatic formation of the excited state. Finally the temperature dependence of CE from the exposure of tungsten to F_2 is modeled utilizing the temperature dependence of the energies for the conduction electrons in the tungsten.

III. EXPERIMENTAL

GAS HANDLING SYSTEM

The experiments were done in an ultra high vacuum system which was equipped with a 240 liter/s triode ion pump. A cryopump was used and the ion pump shut off when gas was being added to the chamber. The gas composition was monitored with a UTI 100C quadrupole mass spectrometer (QMS). Fig. 3.1 illustrates a typical background spectrum during cryopumping at a background pressure of 1×10^{-8} torr. The experimental apparatus is depicted in Fig. 3.2.

XeF_2, F_2 and N_2F_4 were utilized in the gas manifold depending on the valve selected. XeF_2 was obtained from PCR Research Chemicals Inc. and transferred under argon to a stainless steel bottle. The XeF_2 was then vacuum distilled at -64 C to remove excess argon, xenon, and other volatile impurities. The gas flow into a small volume was controlled by a leak valve. The volume pressure was measured with a capacitance manometer which was interfaced with an HP 85B microcomputer. A 1/16 inch stainless steel tube was used to direct a flux of gas leaving the volume toward the sample. The gas conductance of the tube was calculated using Clausing's equation (88):

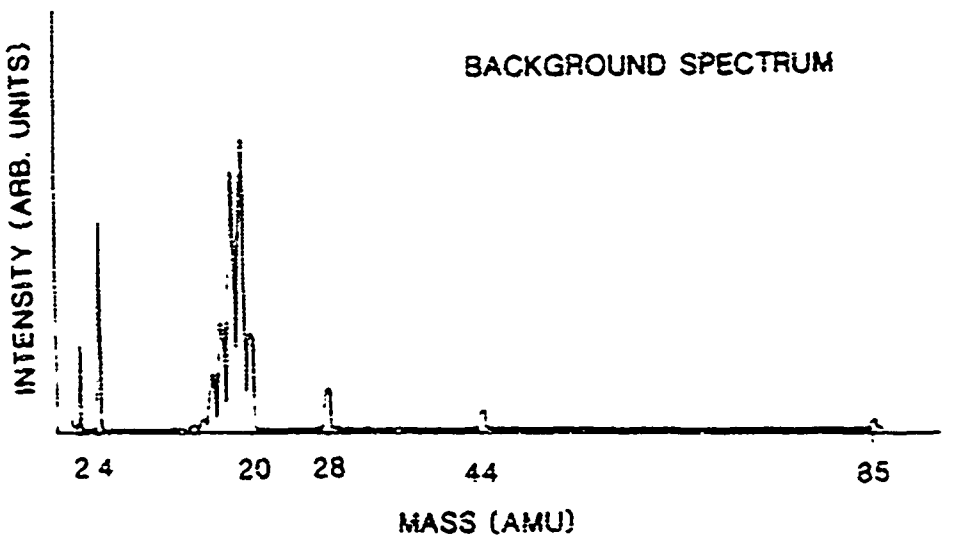

Fig. 3.1 Residual gas background spectrum during cryopumping with an amplification setting of 10^{-7}.

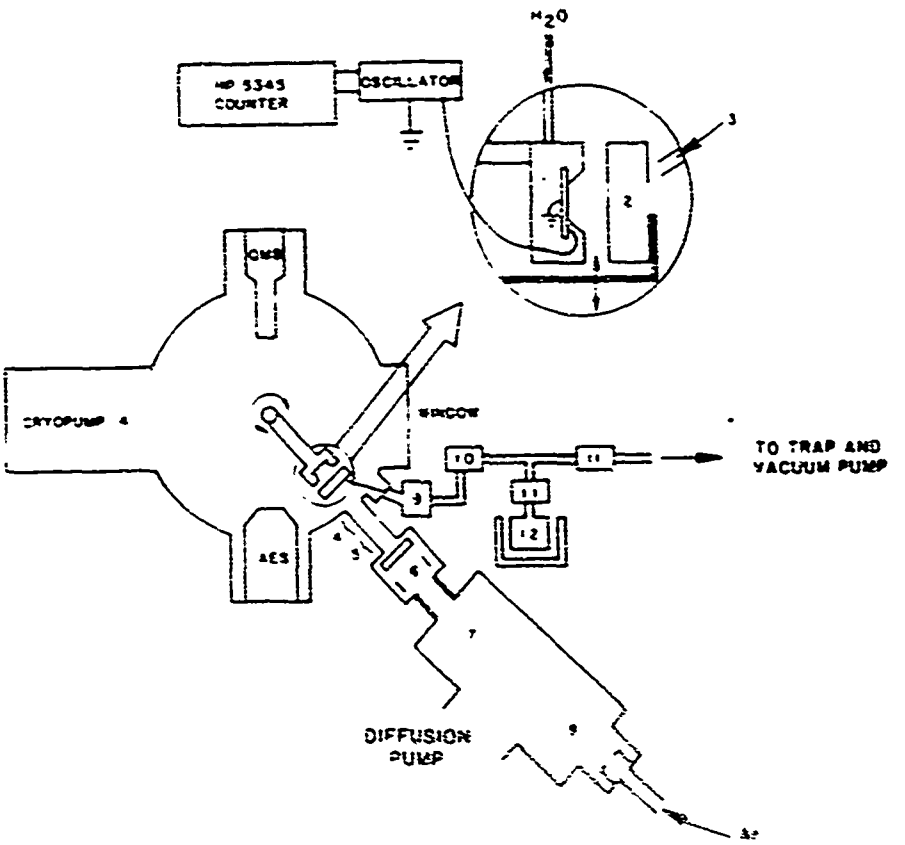

Fig. 3.2 Schematic diagram of experimental apparatus: (1) QCM; (2) Faraday cup; (3) gas dosing tube; (4) in line valve of vacuum isolation; (5) ion decelerator; (6) deflection plates; (7) Wien ion filter; (8) Colutron ion gun; (9) capacitance manometer; (10) leak valve; (11) isolation valves; (12) stainless steel XeF_2 bottle surrounded by dewar for cooling during distillation process.

3.1 $$C = a'vA/4$$

Here, C represents the gas conductance through the tube, A represents the tube's cross sectional area, and a' is Clausing's factor which was taken to be 4d/3l for a long narrow tube (S8). The inner diameter of the tube is d and l is its length. The average velocity of the gas molecules (v) is given by Eq. 3.2 where k is Boltzman's constant, T is temperature, and m is the molecular mass.

3.2 $$v = (8kT/\pi m)^{1/2}$$

The flux of gas (Q) was calculated using Eq. 3.3, assuming the pressure in the chamber is much less than the pressure at the manometer ($P_1 << P_2$).

3.3 $$Q = C(P_2 - P_1) = CP_2$$

The flux was generally maintained at 1×10^{16} molecules/s unless otherwise stated. This condition was met by adjusting the leak valve until the manometer read 0.74 torr with XeF_2 or 0.35 torr with F_2.

The fraction of this flux incident on the sample was calculated assuming the gas leaving the tube follows a $\cos^2(\theta)$ distribution where θ is the angle measured from the direction the tube is pointing. For a majority of

experiments, the sample subtended a solid angle of 1.3 steradians as viewed from the end of the tube. If F is the total flux leaving the tube then the flux hitting the sample is given by Eq. 3.4

3.4
$$F_s = F \frac{\int_0^{0.2} \cos^2 \theta \cdot 2\pi \, d\theta}{\int_0^{\pi/2} \cos^2 \theta \cdot 2\pi \, d\theta} = 0.25 \, F$$

Therefore the average flux of gas hitting the 0.713 cm^2 sample from the tube is maintained at 3.5×10^{15} molecules/cm^2/s.

Fig. 3.3 shows a typical mass spectrum during XeF_2 exposure. The large 19 AMU peak is partially due to a fluorine memory effect which is always present. The large Xe peaks are due to dissociative adsorption of XeF_2 on the surfaces in the chamber. There are two facts which tend to support this. First, our vapor pressure measurements of XeF_2 are very close to 4 torr as reported in the literature (89,90). Second, fast pumping on the XeF_2 with a forepump decreases the XeF^+ peaks at the same rate as the Xe^+ peaks. However, if the flux of XeF_2 into the chamber is increased the XeF^+ peaks increase faster than the Xe^+ peaks, as one would expect if a large portion of the Xe was due to passivation of the chamber walls. Typical XeF_2 spectra in the literature (which we did not attempt to duplicate

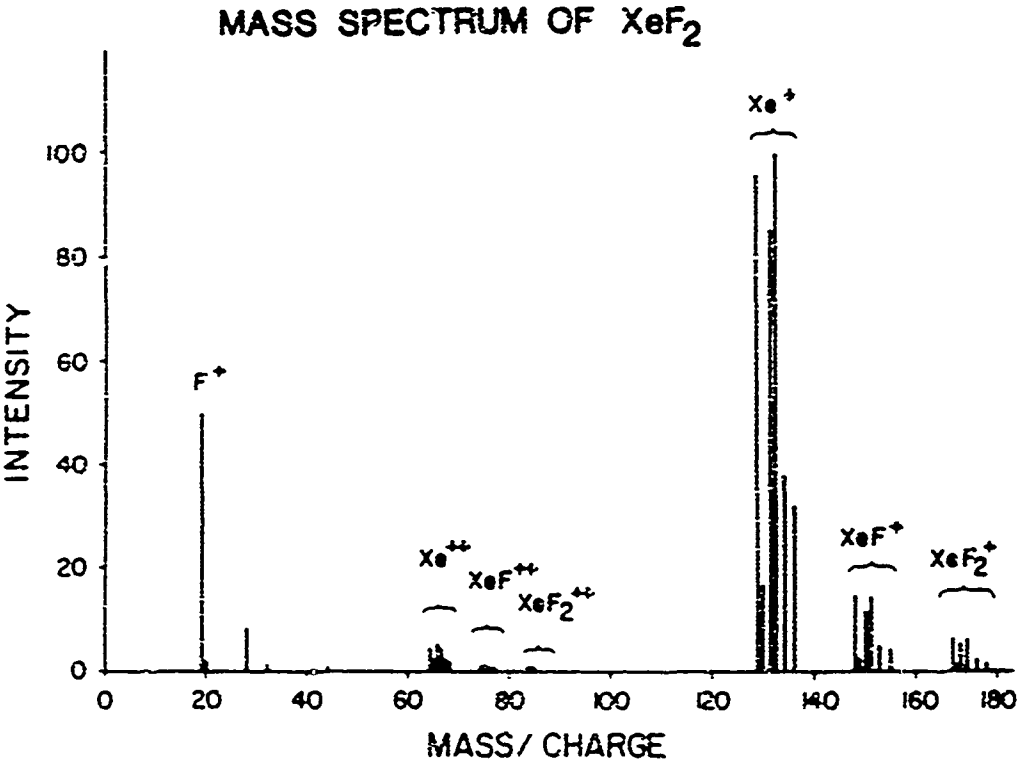

Fig. 3.3 Mass spectrum of XeF_2 plus background taken with EAI QMS.

because of the damage it would have caused to electron multipliers in the chamber) are found in references 89 and 91. The pressure in the chamber as measured with an ion gauge during XeF_2 exposure is 1 X 10^{-5} torr. After the Xe contribution is subtracted out and a correction is made for the ionization cross section for XeF_2 (92), the additional flux of XeF_2 from the background gas during exposure is found to be 7.2 X 10^{13} molecules/cm^2/s. This is negligible compared to the flux from the tube.

A typical mass spectrum during F_2 exposure is shown in Fig. 3.4. The ratio of the intensities of the 38 AMU (F_2^+) to 19 AMU (F^+) peaks is 1.3 in this particular spectrum. This ratio is highly variable and depends on the history of the mass spectrometer ionizer. The ion gauge pressure during F_2 exposure is 2 X 10^{-7} torr. This corresponds to a flux of 4.8 X 10^{13} molecules/cm^2/s. This is negligible compared to the flux from the tube.

AUGER ELECTRON SPECTROSCOPY

The chamber was equipped with a Varian model 981-2607 Auger Electron Spectrometer (AES) which utilizes a Cylindrical Mirror Analizer (CMA). To minimize electron stimulated damage to the surfaces under analysis, a low intensity 2 keV, 0.5 μA incident electron beam was used for AES. Most Auger spectra were obtained with a modulation

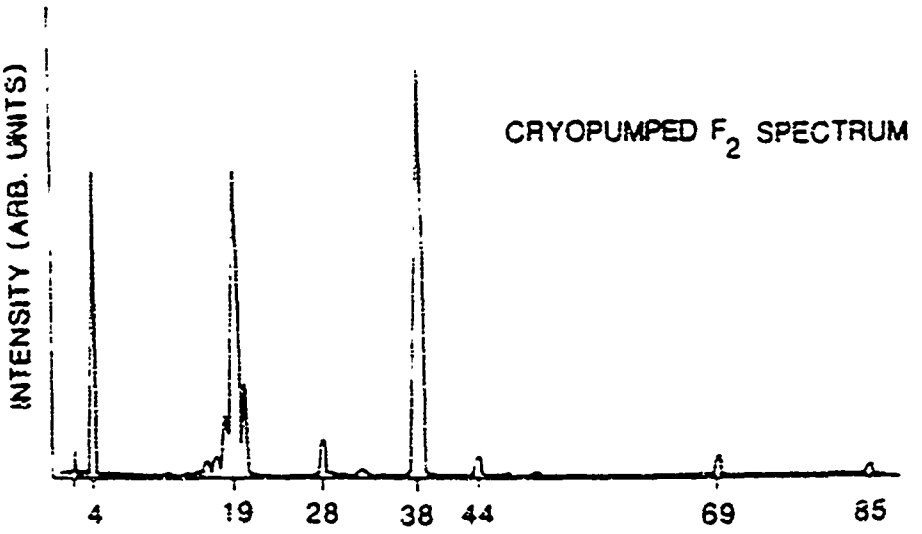

Fig. 3.4 Mass spectrum of F_2 plus background taken with an amplification setting of 10^{-6}.

intensity of 5 V on the CMA and a lock in amplifier set at high sensitivity. The axial electron gun in the spectrometer was used as an electron irradiation source. Its spot size was typically 2.5 mm.

COLUTRON ION GUN

The Colutron ion gun is a differentially pumped, velocity filtered, ion source. It was pumped with a liquid nitrogen trapped 6 inch diffusion pump. The gun consists of a plasma discharge ion source, einsel focusing lens, Wien velocity filter, and a deceleration system. The Wien filter uses crossed electric and magnetic fields to filter the ions. This tends to distort the beam profile. To regain a near gaussian beam profile, electric potentials are applied to a set of 14 metal shims through which the beam passes.

The spot size and shape were first optimized with the aid of a phosphor screen. This was replaced with a Faraday cup to maximize beam current. The composition of the ion beam before filtering was determined by varying the filter parameters. Fig. 3.5 shows the current collected in the Faraday cup as the magnet current in the filter is varied and all other parameters are held constant. Argon gas was being fed into the gun and the ions were being accelerated with 1000 V. Over 95% of the ions from the

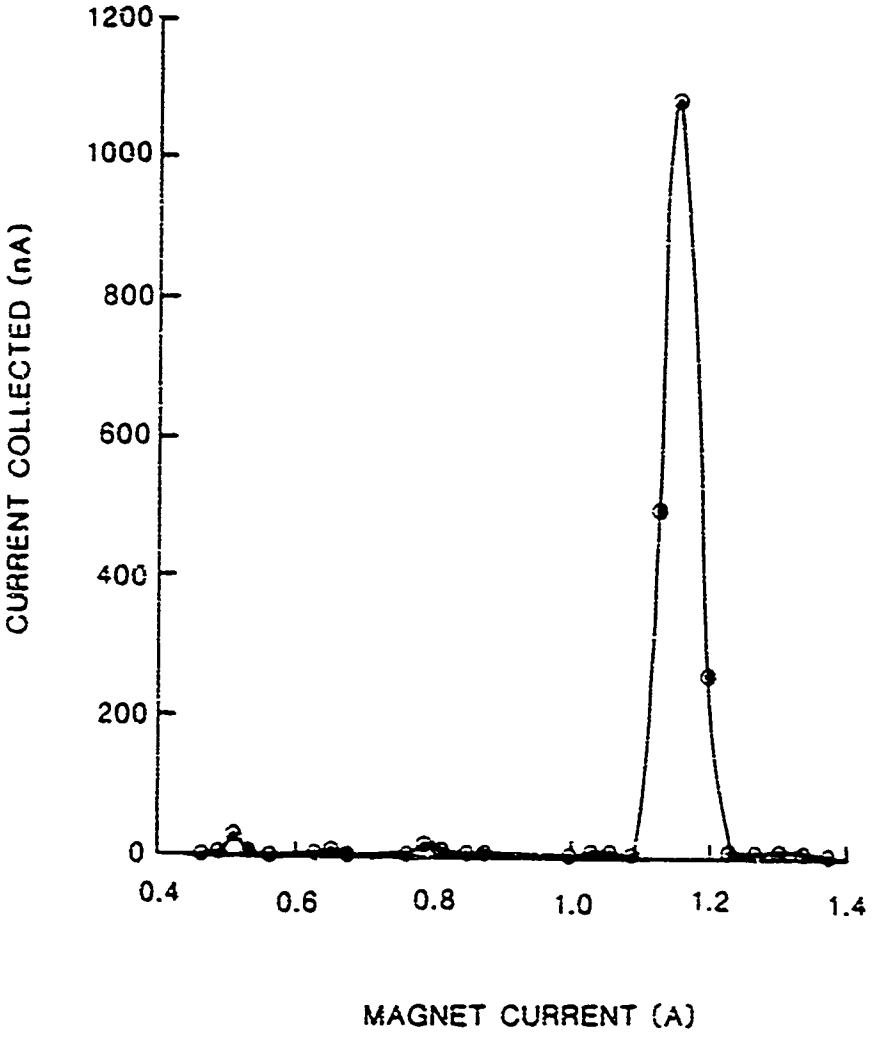

Fig. 3.5 Current collected in Faraday cup as magnet current in Wien filter is Changed. The discharge gas is argon.

argon discharge appear to be Ar^+. However, there is also evidence of Ar^{++} (20 AMU) as well as peaks at 24, 28, 36, and 44 AMU.

QUARTZ CRYSTAL MICROBALANCE

A quartz crystal microbalance was constructed for the purpose of measuring small (monolayer) mass changes. AT cut, 5 MHz. quartz crystals were obtained from Detec. Inc. On each side of the crystal 10 μm of gold or silver were deposited to serve as electrodes. The crystal was placed on an electrically grounded copper block which was cooled by flowing water through it at a rate in excess of 100 ml/min. An electrode made from stainless steel and lava was attached to the other side of the crystal. This electrode had a 5/16 inch hole, which was placed over the center of the crystal and electrically attached to the oscillator as diagrammed in Fig. 3.6. The oscillator is driven at the resonance frequency of the crystal. The signal from the oscillator is fed into an HP 5345A frequency counter which is interfaced with an HP 85B microcomputer for analysis.

The resonance frequency of the thickness shear mode of the quartz crystal is very sensitive to mass loading on one or both sides of the crystal (93). Warner and Stockbridge (94) showed that a change in frequency Δf,

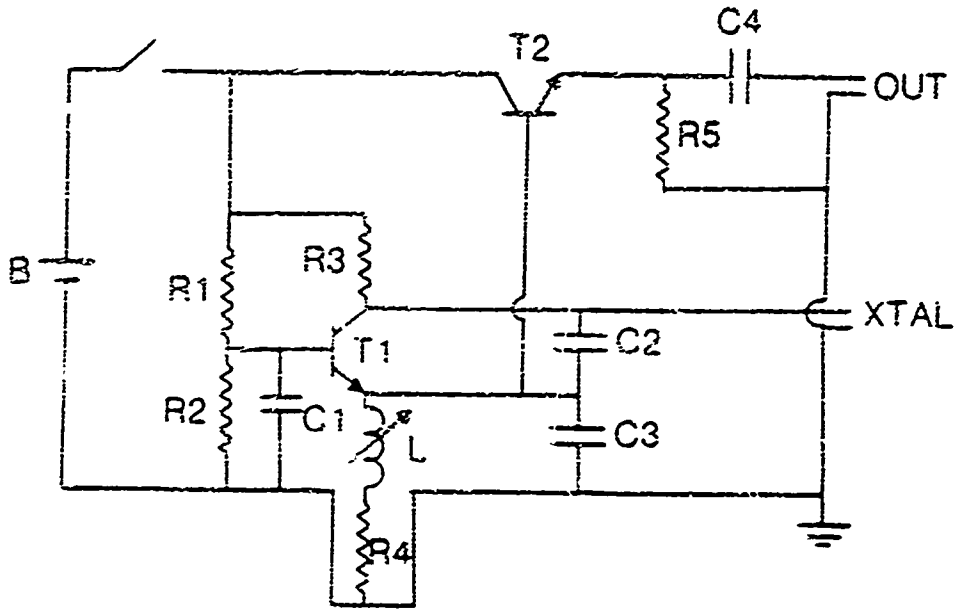

Fig. 3.6 Schematic diagram of oscillator used for QCM. B=22.5 volt battery, C1=0.1 μF, C2=80 pF, C3=160 pF, C4=0.01 μF, L=0.5 mH, R1=20 K, R2=5.1 K, R3=10 K, R4=5.1 K, R5=4.7 K, T1=2N1303, T2=2N3642.

due to a deposit of mass m, added to the area A of the antinodal surface of a quartz crystal resonator is given by

3.5 $$\Delta f = -C_f m/A \quad ;$$
$$C_f = f^2/N\rho_q = 5.65 \times 10^7 \text{ cm}^2/\text{g/s}$$

where ρ_q is the density of quartz, f the resonant frequency of the crystal, and the negative sign implies a decrease in frequency for an increase in mass. The constant N depends on the elastic constants of the crystal and for quartz is given by 1670 mm kHz/s (93). The active surface area of the crystals used here is 0.713 cm^2. Therefore, a frequency increase of 1 Hz would correspond to a mass decrease of 1.26×10^{-8} gram. Very large mass loads, up to 60% of the mass of the quartz crystal itself, can be measured (95). The mass determinations are very accurate and agree to within 1% of the values obtained with other microbalance techniques (96).

Temperature changes and gradients can affect the resonance frequency of the crystals on the order of 3 Hz/C (97). This change varies considerably from crystal to crystal (97). Fig. 3.7 shows the response of the resonance frequency of a crystal to bombardment with a 1 keV, 1 μA electron beam. After 300 s and a frequency increase of 4 Hz, the resonance frequency stabilizes and the QCM stability depends only on the stability of the electron

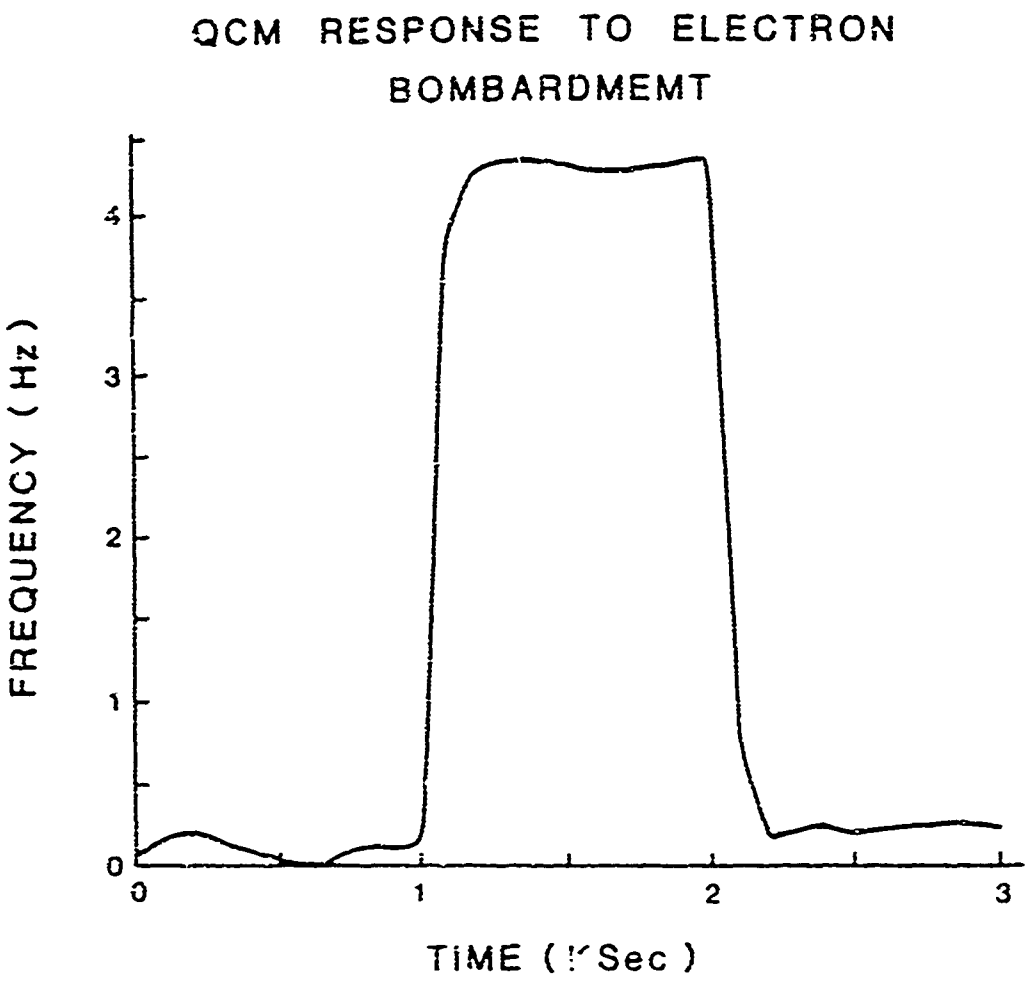

Fig. 3.7 QCM response due to thermal effects caused by a 1 keV, 1 μA electron beam.

gun. After the electron gun is turned off, the resonance frequency returns to the value prior to electron bombardment. The increase in frequency depends linearly on electron current (at constant energy) and electron energy (at constant current) and therefore depends linearly on their product, the incident power. This indicates that the frequency change is due to thermal effects.

The resonance frequency is also dependent upon the pressure and viscosity of the gas in contact with the crystal (98). According to Stockbridge (98), the hydrostatic pressure affects the resonance frequency by 1.35 parts per billion for each torr of pressure. The viscosity of the gas affects the pressure according to Eq. 3.6.

$$(\Delta f/f)_v = 7.2 \times 10^{-7} (f \eta_g \rho_g)^{1/2} \quad ; \quad \rho_g = Pm/RT \tag{3.6}$$

where η_g is the viscosity of the gas and ρ_g its density. Note the dependence on (pressure)$^{1/2}$. The combination of these 2 effects in 1 torr of air amounts to a change in the resonance frequency of -0.02 Hz. In 1 torr of F_2 and XeF_2 this amounts to -0.03 Hz and -0.04 Hz respectively. These changes are negligible compared to the changes in resonance frequency which were measured.

The mass sensitivity of the quartz crystals has a

spatial dependence on the surface of the crystal. The crystal is more sensitive in the center than near the edge. Fig. 3.8 shows the response of a crystal to sweeping an electron beam across the surface. Care was taken during electron bombardment experiments to focus the beam in the central 1 cm "active area" of the crystal. During ion bombardment and sorption studies, the entire face of the crystal was exposed and thus the mass change measurements reported may be somewhat too small in these cases.

THIN FILM COATINGS

Thin film coatings were deposited on quartz crystals at the Naval Weapons Center at China Lake and shipped to WSU under nitrogen. All films were 1000 A thick. SiO_2 films were sputtered onto the quartz crystals using a Perkin-Elmer 6 inch RF sputtering system. From a base pressure of 2×10^{-7} torr, oxygen was bled in to 1×10^{-4} torr and argon was bled in until a pressure of 8×10^{-3} torr was reached. The sputtering system was operated at 500 W for 10 minutes. ThF_4, MgF_2, and Al_2O_3 films were thermally evaporated onto quartz crystals. The ThF_4 films studied in Section VI were evaporated onto a gold substrate at a rate of 3 A/s. The substrate temperature was held at 150 C, and the background pressure was 9×10^{-8} torr during evaporation.

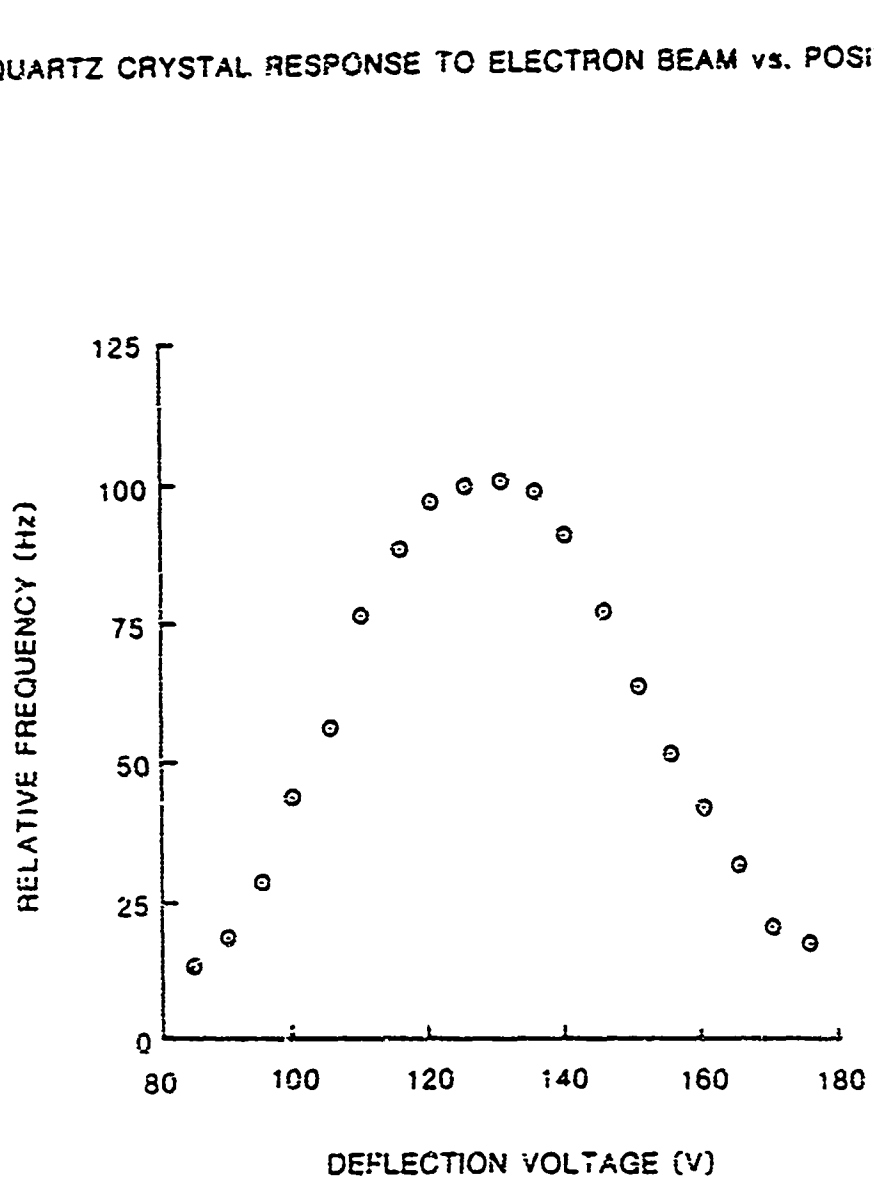

Fig. 3.8 QCM response to sweeping an electron beam across one face of the crystal.

FARADAY CUP

A Faraday cup was constructed to measure the intensity of charged particle beams. It could be moved in front of the microbalance as indicated in Fig. 3.2. The Faraday cup was constructed with a stainless steel collector housed in, and insulated from, a stainless steel enclosure. A 5/16 inch hole in one side of the enclosure, which was covered with a high transparency grid, allowed entry of the charged particles into the Faraday cup. The collector was fixed at a potential such that secondary charged particles would be deflected from the grid over the hole back onto the collector. Fig. 3.9 shows the dependence of current collected from a 1 keV electron beam vs. the positive potential applied to the collector. The Faraday cup was operated at 20 V for electron detection. For positive ion detection, the current with no bias on the Faraday cup was measured. This is assumed to be I^++N-P, where I^+ is the ion current in the primary beam, N is the negative secondary particle current (electrons and ions), and P is the positive secondary ion current. When the Faraday cup was biased positive to saturation, the negative secondary particles were collected and I^+-P was measured. When the Faraday cup was biased negatively to saturation, the positive secondary ions were collected and I^++N was measured. From these three equations, the ion current

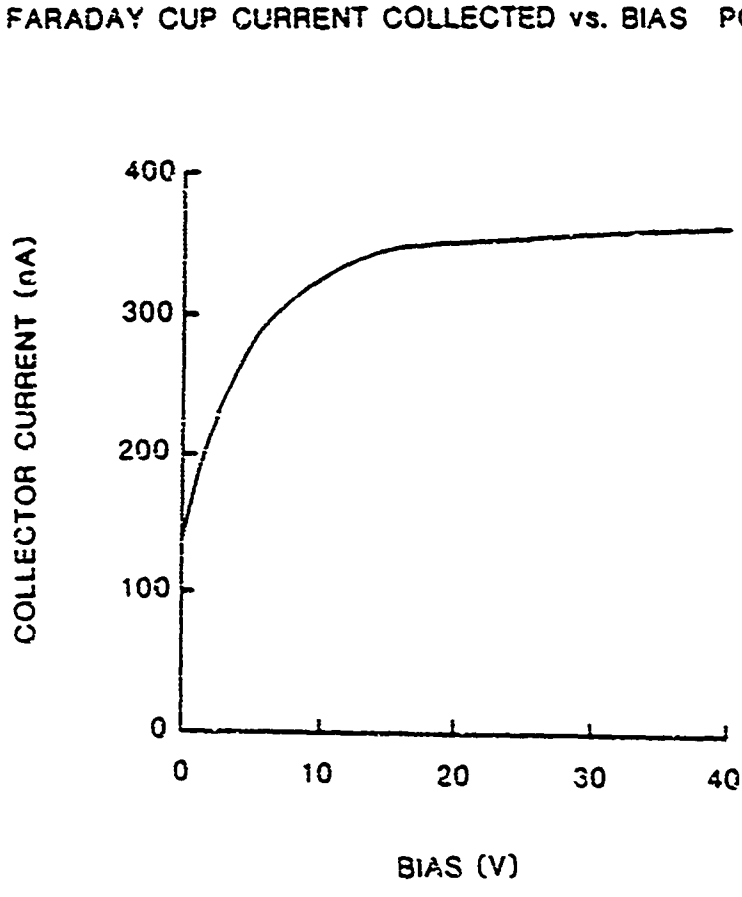

Fig. 3.9 Current collected by the Faraday cup collector from a 1 KeV electron beam as the collector voltage is changed.

could be determined. The positive and secondary ion yields on the stainless steel collector could also be measured (P/I^+ and N/I^+ respectively). These can be used to more accurately determine the ion current at the location of the microbalance by replacing the quartz crystal with a stainless steel plate.

CHEMI-EMISSION DETECTION

Electron emission was detected with a Galileo 4039 Channel Electron Multiplier (CEM). The CEM shown in Fig. 3.10 was operated at 2.5 kV. The pulses were amplified, discriminated, and counted. The count rate was recorded simultaneously with the pressures behind the gas dosing tube by an HP 85B microcomputer. Photoelectrons generated in the chamber by shining an incandescent light through a pyrex window were used to check the gain and sensitivity of the CEM. During the experiments the window was covered to eliminate unwanted counts.

The sample consisted of a 14 cm length of 14 um diameter polycrystalline tungsten wire wrapped into a spiral filament 0.15 cm in diameter. The ends of the filament were spot welded to high current stainless steel leads. The tungsten samples were heated resistively and the temperature was determined by measuring the resistivity. At high temperature, the temperatures

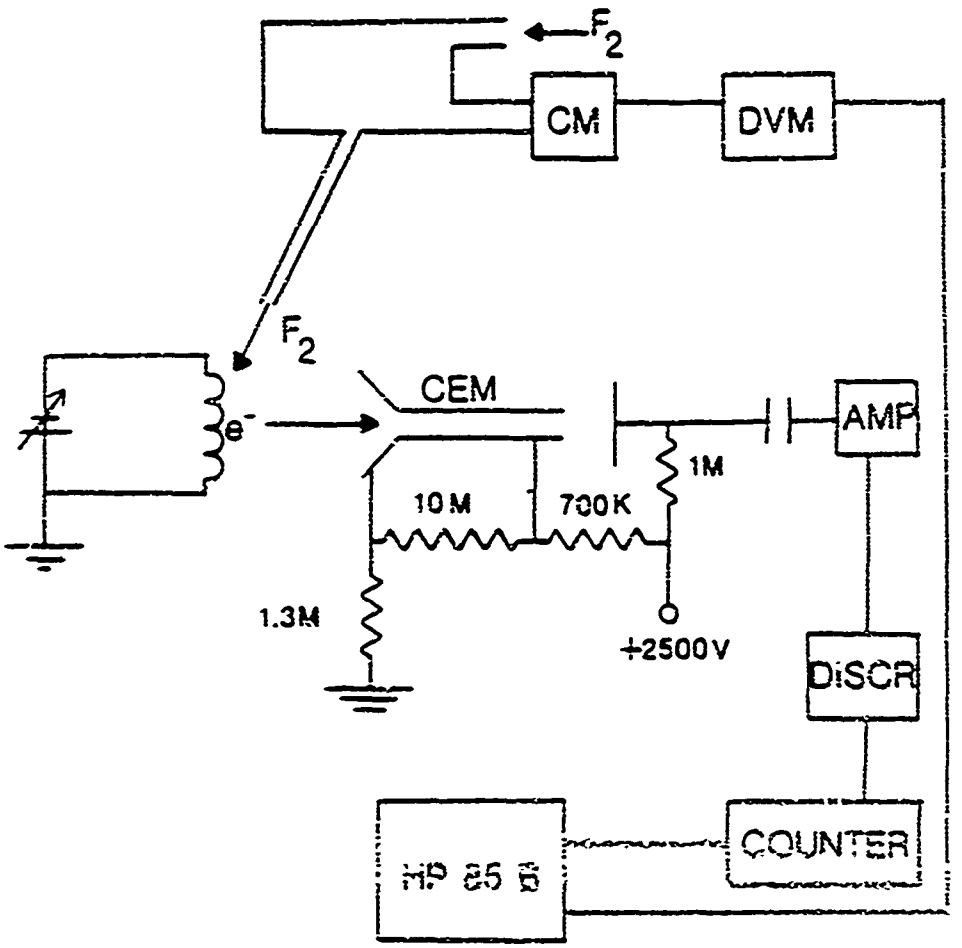

Fig. 3.10 Experimental apparatus used to simultaneously measure CE and incident gas flux.

obtained by resistivity measurements agree with those obtained with optical pyrometry to within 15 C.

The sample was cleaned by numerous resistive heatings to 2800 C followed by F_2 exposure. Exposure to F_2 conveniently removed an oxygen contaminant, presumably tungsten oxide (98,99). AES revealed a large oxygen concentration on the surface following long exposure to background gases and before fluorine exposure. After fluorine exposure a single flashing to 2500 C was sufficient to obtain a clean surface. To minimize contamination from background gases (including F_2), experiments were performed immediately after flashing.

IV. THE CHEMICAL SPUTTERING OF SILICA BY Ar^+ IONS AND XeF_2

When an SiO_2 thin film was exposed to XeF_2, QCM registered a mass increase (frequency decrease) as shown in Fig. 4.1. AES revealed the presence of fluorine after exposure as shown in Fig. 4.2. No adsorbed xenon was observed with AES. The microbalance frequency change during the adsorption corresponded to 2.5×10^{-8} gm (approximately one monolayer of fluorine). During the initial adsorption of fluorine onto the surface, one half of the monolayer is adsorbed in the first 5 minutes. A sticking coefficient of 0.14 was measured during the first 5 minutes. After this time, the adsorption rate per available site declines, indicating a decrease in the sticking coefficient. After a monolayer of fluorine is adsorbed, there is no further mass change, indicating that a spontaneous reaction between the surface of our SiO_2 films and XeF_2 leading to a volatile product such as SiF_4 does not occur, as shown previously by Coburn and Winters (19).

The physical sputtering rate of the SiO_2 with a 0.83 uA, 500 eV Ar ion beam was measured to be 1.0 Hz/min which corresponds to 24 AMU/Ar ion. This etch rate can be seen at the beginning of Fig. 4.3. This physical sputtering yield was measured in a vacuum of 2×10^{-7} torr.

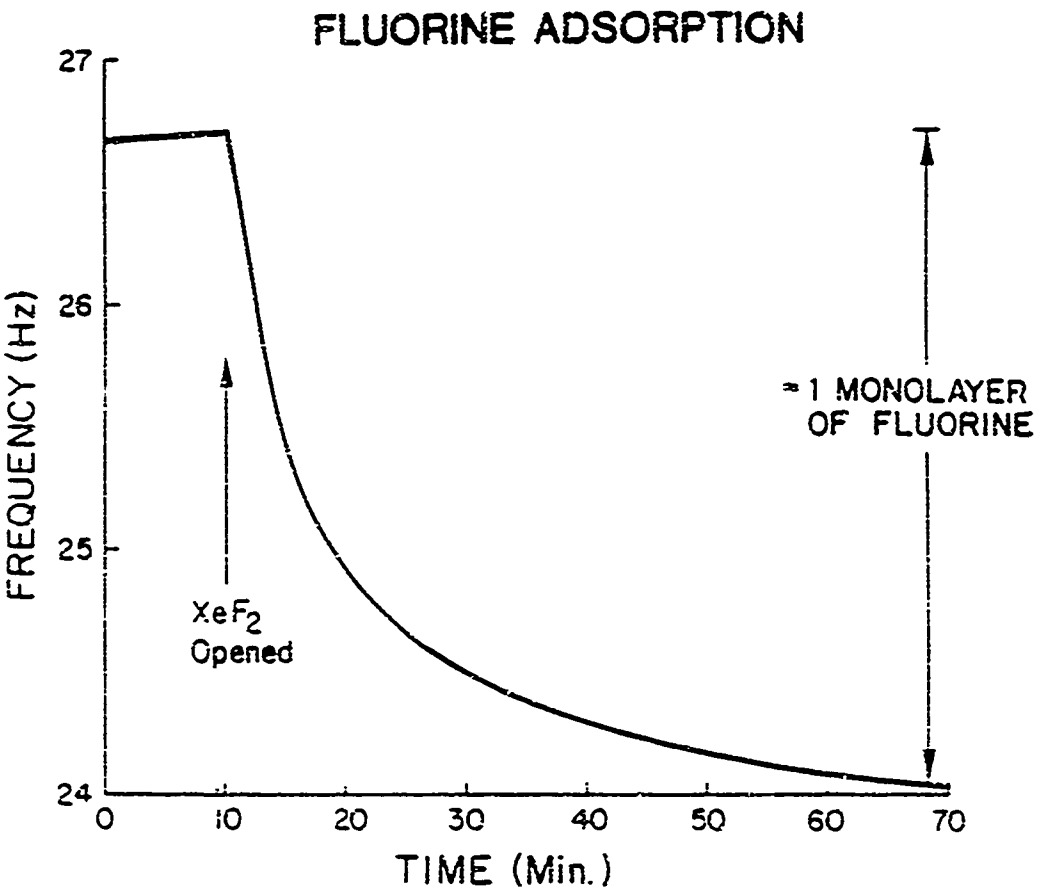

Fig. 4.1 QCM response during the initial adsorptior of fluorine on an SiO_2 thin film during XeF_2 exposure.

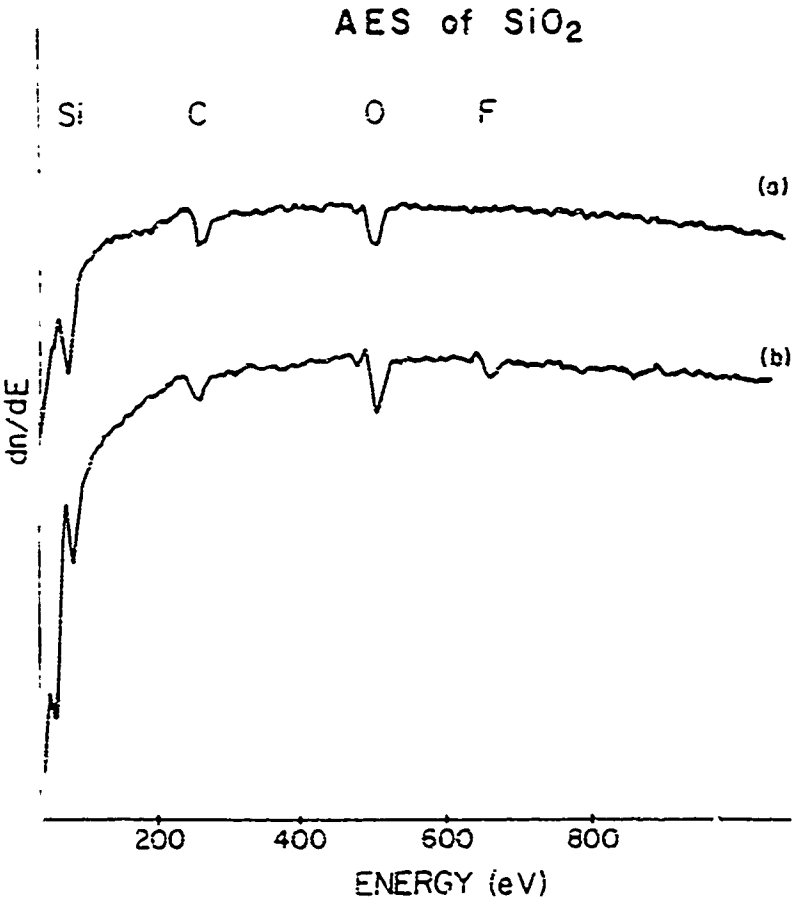

Fig. 4.2 AES of silica film (a) before and (b) after exposure to XeF_2.

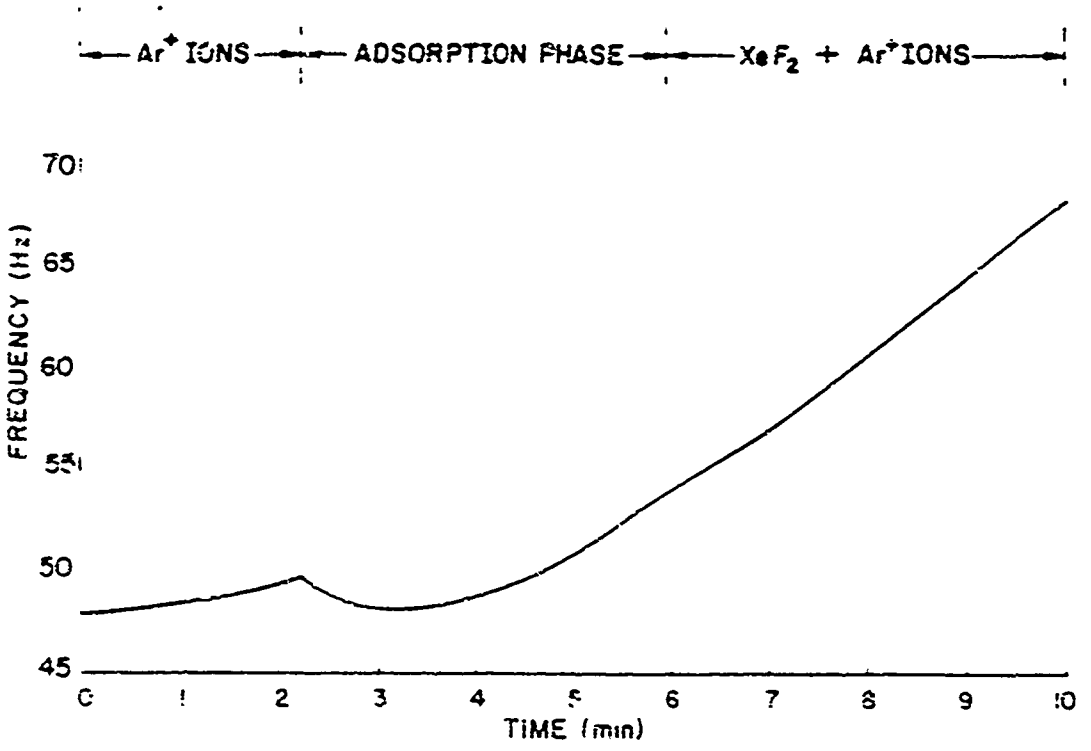

Fig. 4.3 QCM response taken during 500 eV Ar ion bombardment with constant ion gun parameters. XeF_2 was admitted to the system at t=2 min.

Most of this (approximately 1.7 X 10^{-7} torr) was argon from the ion source. Some residual fluorine was present in the background gases which may account for our slightly larger physical sputtering yield when compared to other published values (8,36). However, our value agrees well with the value of Tu et. al. (8) who obtained 0.3 molecules/ion which we interpret as 20 AMU/ion. Our value also agrees well with the value published by Zalm et. al. (36) of 0.6 atom/ion which we interpret as 12 AMU/ion.

When XeF_2 was allowed into the dosing tube while the sample was being physically sputtered (shown in Fig. 4.3), the SiO_2 surface initially went through an adsorption phase. After 4 minutes, equilibrium was reestablished with the SiO_2 etching at the much faster rate of 3.5 Hz/min which corresponds to 86 AMU/Ar ion. During adsorption, a surprising amount of mass was gained before mass loss resumed. This mass corresponds to 0.8 monolayer of fluorine adsorbed. This suggests that a large fluorine coverage is necessary for a large enhancement in the etch rate.

We studied the SiO_2-F adsorbate system by allowing fluorine to adsorb onto the SiO_2 from XeF_2 and then pumping the XeF_2 away. After pumpout, the SiO_2-F(ads) surface was irradiated with the Ar ion beam. Fig. 4.4 is the response of the QCM when this sample was suddenly subjected to Ar ion bombardment. The etch rate can be obtained by

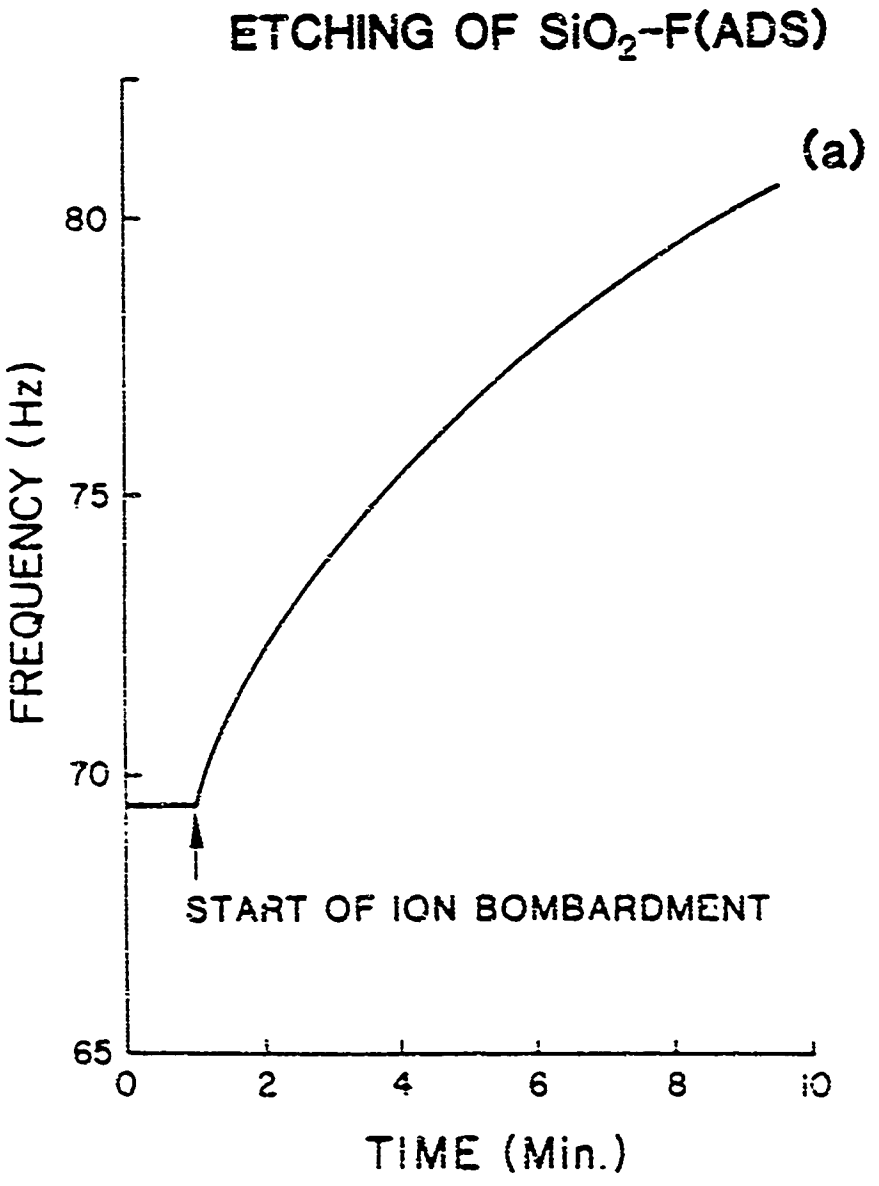

Fig. 4.4 QCM data of SiO_2 - F adsorbate behavior when suddenly subjected to Ar ion bombardment at 1×10^{-8} torr.

differentiating the total mass gain in Fig. 4.4, and is shown in Fig. 4.5. The results clearly indicated the enhanced etching behavior during the initial bombardment. For early times, the etch rate was identical to that observed with both ion bombardment and XeF_2 exposure. As the adsorbate and the reaction products were sputtered off, the etch rate declined to the physical sputtering rate.

The enhanced etch rate obtained with the pre-adsorbed fluorine layer in vacuum clearly demonstrates that it is the adsorbate that is responsible for the enhanced etching behavior. If we assume that the products of chemical sputtering of SiO_2 are primarily SiF_4 and O_2 (101), then we can calculate the number of SiO_2 molecules chemically sputtered by the monolayer of adsorbed fluorine. Integrating the curve in Fig. 4.5 for the first 4 minutes and subtracting the portion due to physical sputtering, we obtain approximately 0.8 monolayer of SiO_2. We can conclude that had the fluorine coverage not decreased during this time, then one monolayer of fluorine would have been responsible for removing approximately one monolayer of SiO_2.

As this work indicates, fluorine adsorption is a necessary step for the chemical sputtering of SiO_2 with XeF_2. However, one must then ask what is the role of the ion beam? The Ar ions can sputter away the loosely bound reaction products (e. g., SiF_4) (19) leaving new SiO_2

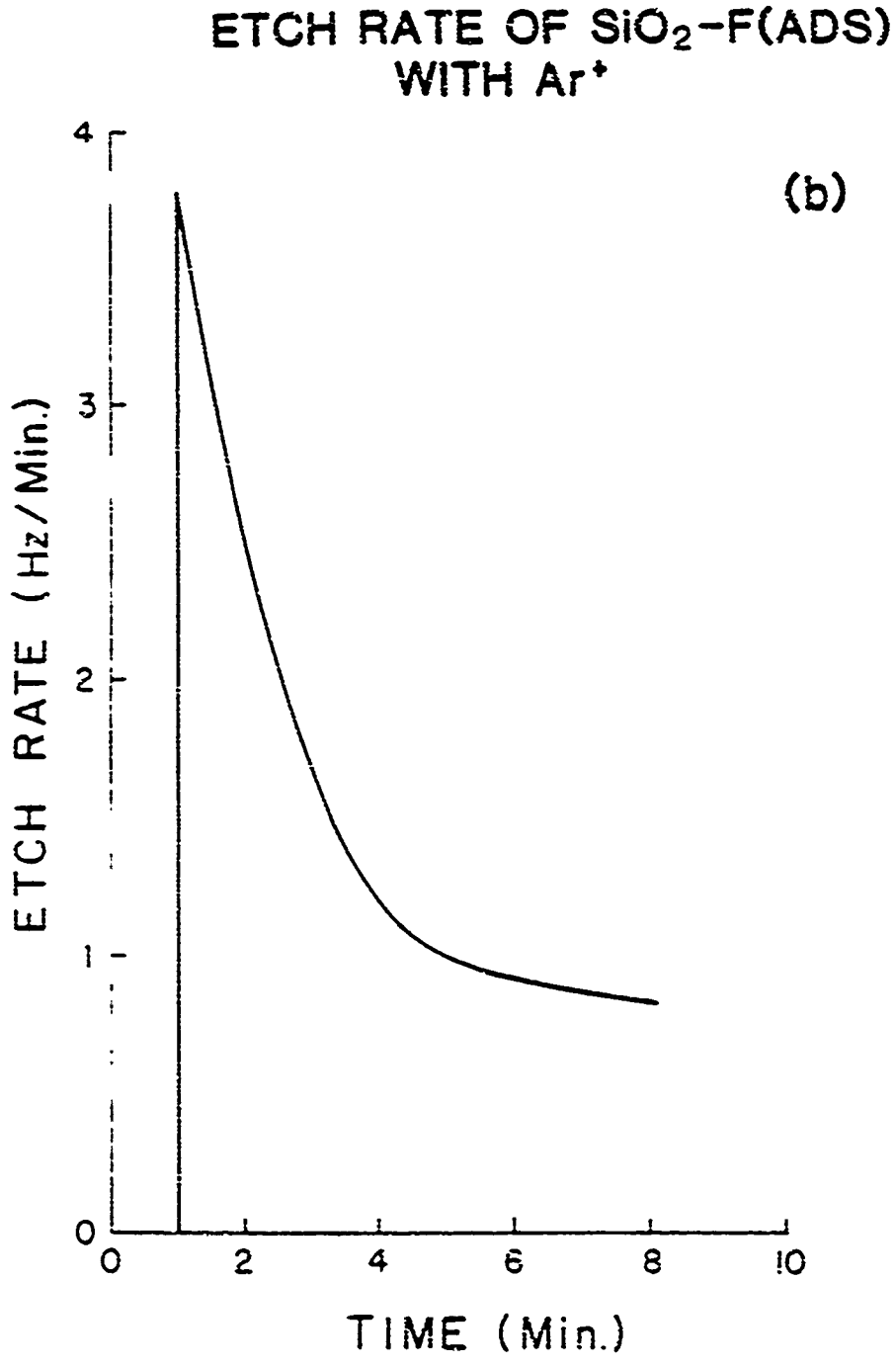

Fig. 4.5 Etch rate of the SiO_2 - F(ads) surface during Ar ion bombardment at 1 X 10^{-8} torr.

available to adsorb more fluorine. The ions may also stimulate the chemical reaction by rearranging the surface constituent atoms from their room temperature equilibrium positions (6) or by supplying energy to overcome activation barriers (8).

V. ELECTRON ENHANCED SORPTION OF FLUORINE BY SILVER SURFACES

INTRODUCTION

Electron stimulated desorption (ESD) is a common occurrence when an adsorbate covered surface is subjected to electron bombardment (71, 74-76, 77, 82, 110, 111). Other electron stimulated phenomena include dissociation of the adsorbate and its chemical reaction with the substrate (17, 18, 41, 79, 83, 84). However, minimal information exists on electron stimulated absorption of an adsorbate into the bulk of a substrate and subsequent chemical reactions. This may be due in part to the difficulty of detecting an atom in the bulk compared to the relative ease of detecting a desorbed particle in the gas phase or determining the chemical nature of the atomic species on a surface. We have found that a quartz crystal microbalance (QCM) serves well to measure mass increases due to the adsorption, absorption and subsequent reaction with surfaces exposed to fluorine containing gases. In addition, we can readily observe the consequences of simultaneous electron bombardment on the rate of mass gain or loss.

The QCM is often used to measure mass changes of thin films in fluorine containing environments (3, 8, 19,

55). Usually silver electrodes are evaporated onto the quartz crystal and the thin film to be investigated is deposited on top of one of these electrodes. Often portions of the silver electrodes are exposed to the fluorine containing gases and may be a major source of error in these measurements. In addition, our measurements also suggest that fluorine may find its way through several such thin film overlayers (SiO_2, Al_2O_3, MgF_2, and ThF_4) to reach and react with the underlying silver surface, encouraging further uptake of gas. In contrast, when gold is used as an electrode material, we have not observed more than a monolayer of fluorine adsorption.

This work bears directly on coatings technology where protection of underlying surfaces is desired. In addition, electron stimulated diffusion and electron stimulated chemical reactions may be useful tools in the preparation and doping of thin films.

EXPERIMENTAL

The experiments were done in a stainless steel UHV chamber equipped with a 220 l/s ion pump and a cryopump. The base pressure of the system was 1 X 10^{-8} torr without baking. Gaseous XeF_2 and F_2 were directed at the samples by means of a 1/16 inch stainless steel dosing tube. A capacitance manometer measured the pressure of the gas as

it entered the dosing tube and together with the calculated gas conductance of the tube allowed us to calculate the flux of molecules exiting the doser. The pressure of the gas behind the dosing tube was adjusted such that the flux of molecules exiting the doser was maintained at 1 X 10^{16} molecules/s for both F_2 and XeF_2. The flux density incident on the 0.71 cm^2 active area of the quartz crystal was calculated to be 3.5 X 10^{15} molecules/s.

Mass changes were detected with a thermally stabilized QCM. Silver or gold coated 5 MHz crystals were obtained from Detec Inc. The resonance frequencies of the crystals were measured with an HP 5345A electronic counter and analyzed with an HP 85B microcomputer. For this QCM, a frequency increase of 1 Hz corresponds to a mass decrease of 12.6 X 10^{-9} grams (102).

The residual gas composition was measured with a quadrupole mass spectrometer (EMI QUAD 160). Auger Electron Spectroscopy (AES) was done with a Varian Auger Cylindrical Mirror Analyzer(CMA). The electron source used for this study was the axial Auger electron gun in the CMA. This equipment is described further in reference.

RESULTS AND DISCUSSION

SPONTANEOUS GROWTH OF SILVER FLOURIDE

No attempt was made to clean the silver surfaces prior to gas exposure. AES of the silver surface revealed a trace of carbon after pumpdown. The carbon was diminished after exposure to F_2 or XeF_2 and completely disappeared after simultaneous exposure to F_2 or XeF_2 and electrons.

When a silver surface was exposed to F_2, a layer of fluorine was adsorbed onto the surface. Fig. 5.1 shows the F_2 adsorption-induced frequency shift of the monitoring crystal after F_2 was introduced to the sample at the time indicated. The resonance frequency of the crystal dropped 2.58 Hz during the first 600 seconds of adsorption. This corresponds to a mass gain of 3.25×10^{-8} grams or 0.85 monolayer of fluorine (one monolayer corresponds to 1.1×10^{15} silver atoms/cm^2). From the first 200 seconds of adsorption an average sticking coefficient of 0.016 was calculated (assuming the adsorption sites are being filled from the gas phase faster than they are being vacated by adsorbed atoms diffusing into the bulk). After 0.85 monolayer of fluorine was adsorbed the silver surface continued to gain mass from the fluorine gas at a constant rate of 3.0×10^{-11} grams/s which corresponds to

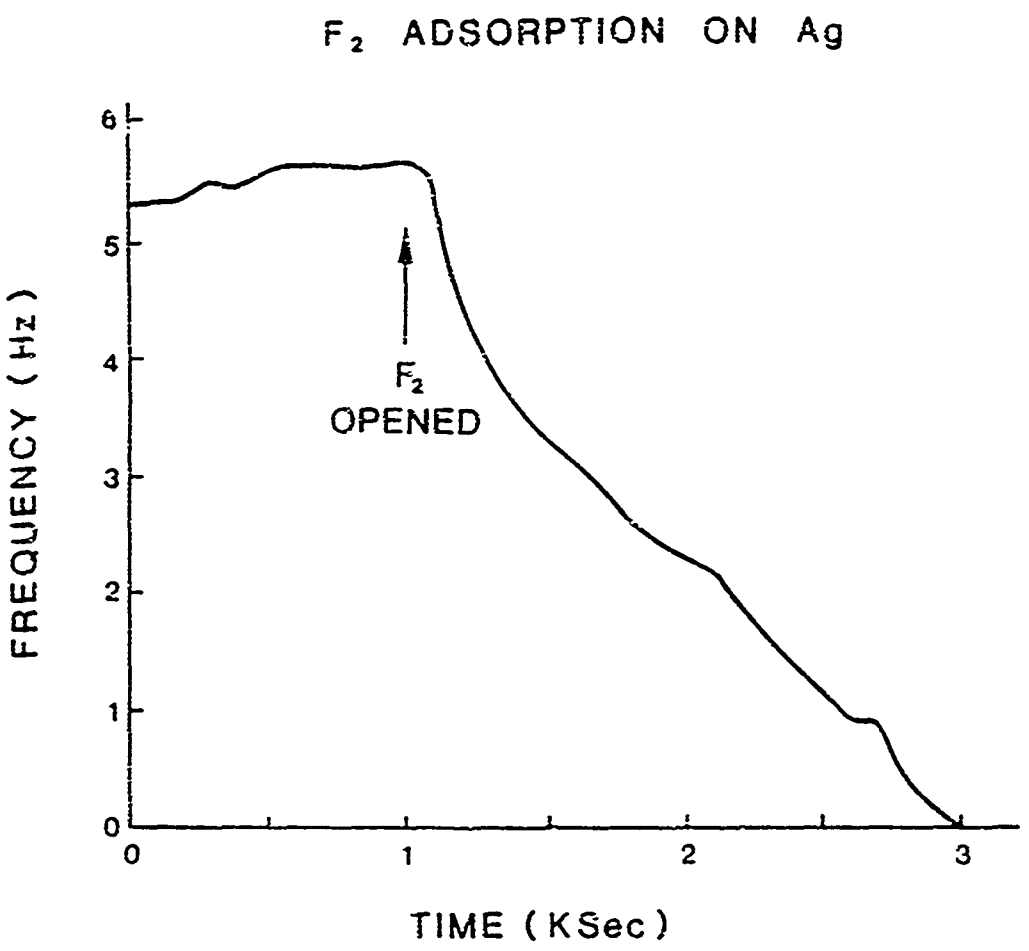

Fig. 5.1 QCM response to exposure of a pristine silver surface to F_2.

approximately 7 X 10^{-4} monolayer/s. Over long periods of time the rate of mass uptake did not appear to change significantly. When the flux of F_2 to the surface was increased by up to a factor of 2, the mass uptake was found to increase approximately in proportion to the flux.

In a similar fashion, when a fresh silver surface was exposed to XeF_2 a layer of fluorine was initially adsorbed onto the surface. In Fig. 5.2 we plot the QCM response during XeF_2 exposure. After exposure to XeF_2 at the time indicated, the resonance frequency of the crystal drops 3.74 Hz in the following 400 s. This corresponds to 4.7 X 10^{-8} grams (1.1 monolayer of fluorine). For the first 200 s of adsorption a sticking coefficient of 0.02 is calculated. Thereafter the silver surface continues to gain mass from the XeF_2 at a constant rate of 2.0 X 10^{-11} grams/s (4.5 X 10^{-4} monolayer/s).

Fig. 5.3 shows the behavior of the resonance frequency of the QCM when the silver surface is subjected to a large flux of XeF_2. At the time indicated, the XeF_2 flux is doubled to 2 X 10^{16} molecules/s. Immediately the rate of mass gain increases by a factor of 2. At t = 4600 s, at which time the total mass gain is equivalent to 3.8 monolayer, the mass gain rate starts to accelerate. This acceleration proceeds until at t = 6500 s (9.8 monolayers) a mass gain rate of 2.8 X 10^{-10} grams/s (6.5 X 10^{-3} monolayer/s) is established. This is a seven fold

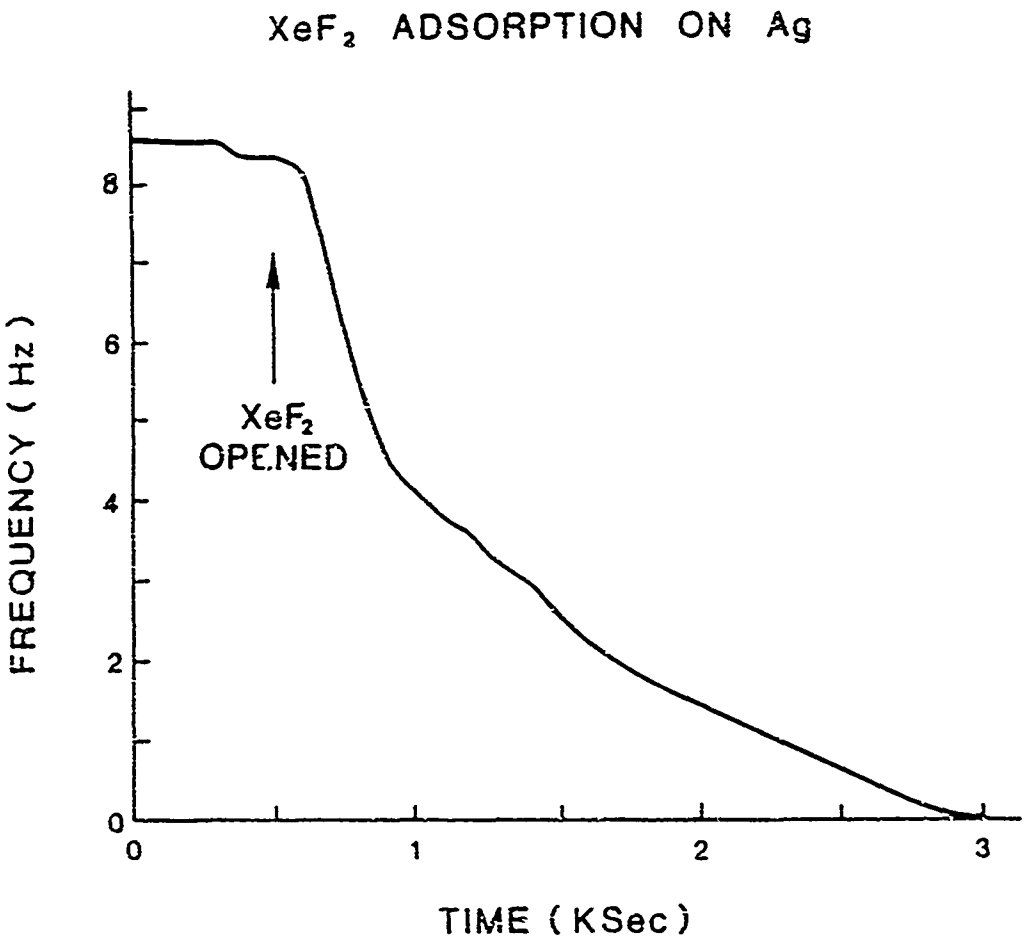

Fig. 5.2 QCM behavior when the silver surface is exposed to XeF_2.

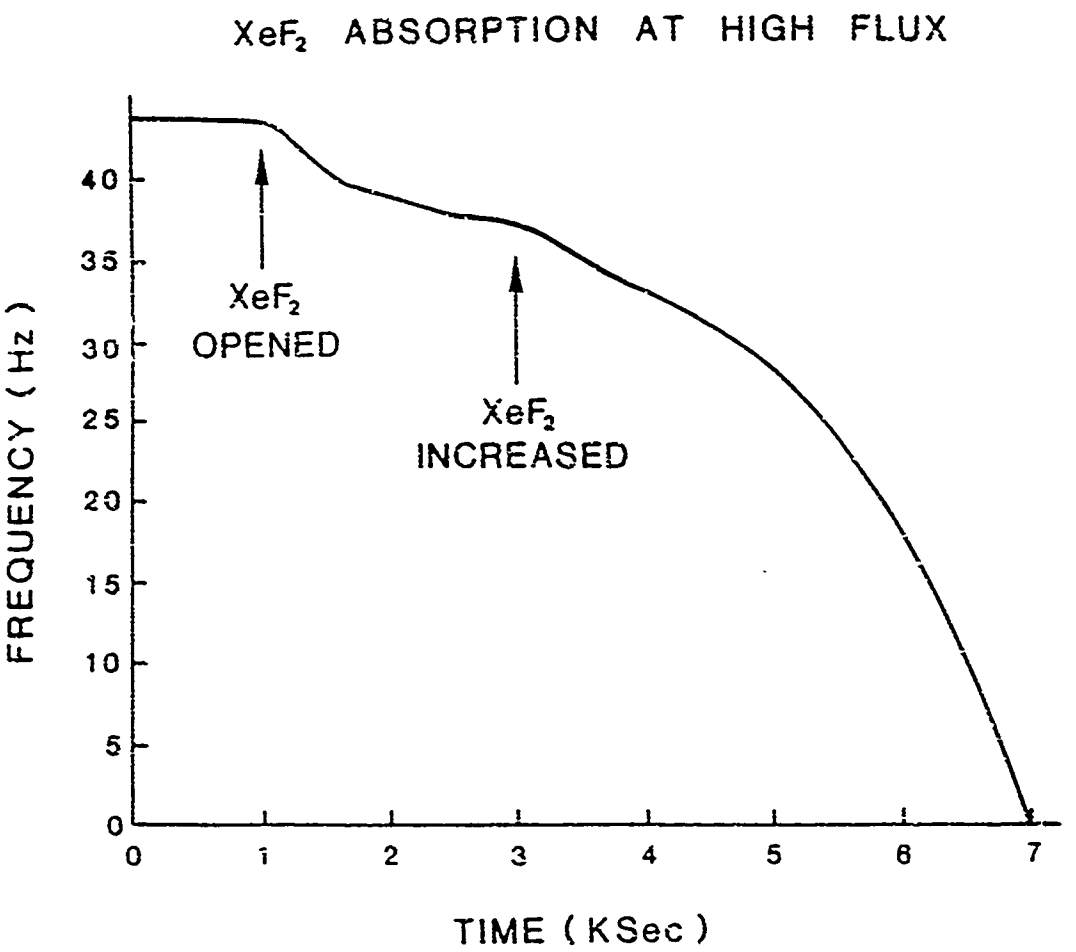

Fig. 5.3 QCM response when the silver surface is subjected to a large flux of XeF_2.

increase. At this high rate of gas uptake one would expect a large concentration of fluorine in the near surface layers. This is verified by AES. Indeed the surface layers resemble silver fluoride more than silver. For sufficient fluorine exposure, the surface of the silver turns a distinct brown color which is an indication that AgF has been formed. We conclude that fluorine adsorption and silver fluoride growth occurs at a higher rate for a silver fluoride surface exposed to XeF_2, as opposed to a silver surface. The fact that this does not occur with F_2 indicates that it is not a bulk effect, if one assumes that the same surface species results from F_2 and XeF_2 adsorption. This behavior can be explained by the presence of a more mobile species resulting from the adsorption of XeF_2 onto a silver fluoride surface.

McIntyre et. al. (102) have observed similar rapid AgF formation when a silver surface was exposed to atomic fluorine from a discharge. Due to the unstable nature of XeF_2 it would seem plausible to conclude that XeF_2 dissociatively chemisorbs on a silver fluoride surface resulting in at least a partial layer of atomic fluorine, which diffuses to and reacts more readily with the underlying silver.

SILVER FLOURIDE GROWTH UNDER ELECTRON BOMBARDMENT

When a beam of electrons is incident on a quartz crystal, thermal gradients are created which can cause frequency shifts. Fig. 5.4 shows the response of the crystal to the thermal gradient created by a 1 KeV, 1 uA electron beam incident on one face of the crystal. Note from Fig. 5.4 that the frequency reaches equilibrium within 300 s after initiation and termination of electron bombardment.

A 1 KeV, 5 uA electron beam was found to significantly enhance the rate of fluorine uptake in F_2. A comparison of Fig. 5.5 with Fig. 5.1 bears this out. Data in Fig. 5.5 were obtained under identical conditions as in Fig. 5.1 except for the presence of the electron beam as indicated. The rate of mass gain during this time remains a steady 9.37×10^{-11} grams/s or 2.3×10^{-3} monolayer/s. This represents an over 3 fold enhancement in the fluorine uptake rate.

An even larger fluorine uptake rate can be obtained from the combination of XeF_2 and electron bombardment on the silver surface. The QCM data of Fig. 5.6 was obtained with the same XeF_2 flux as in Fig. 5.2, the only difference again being the presence of the 1 KeV, 5 uA electron beam during the times indicated. From a mass gain rate of 2.0×10^{-11} grams/s (4.6×10^{-4} monolayer/s) the rate of fluoride

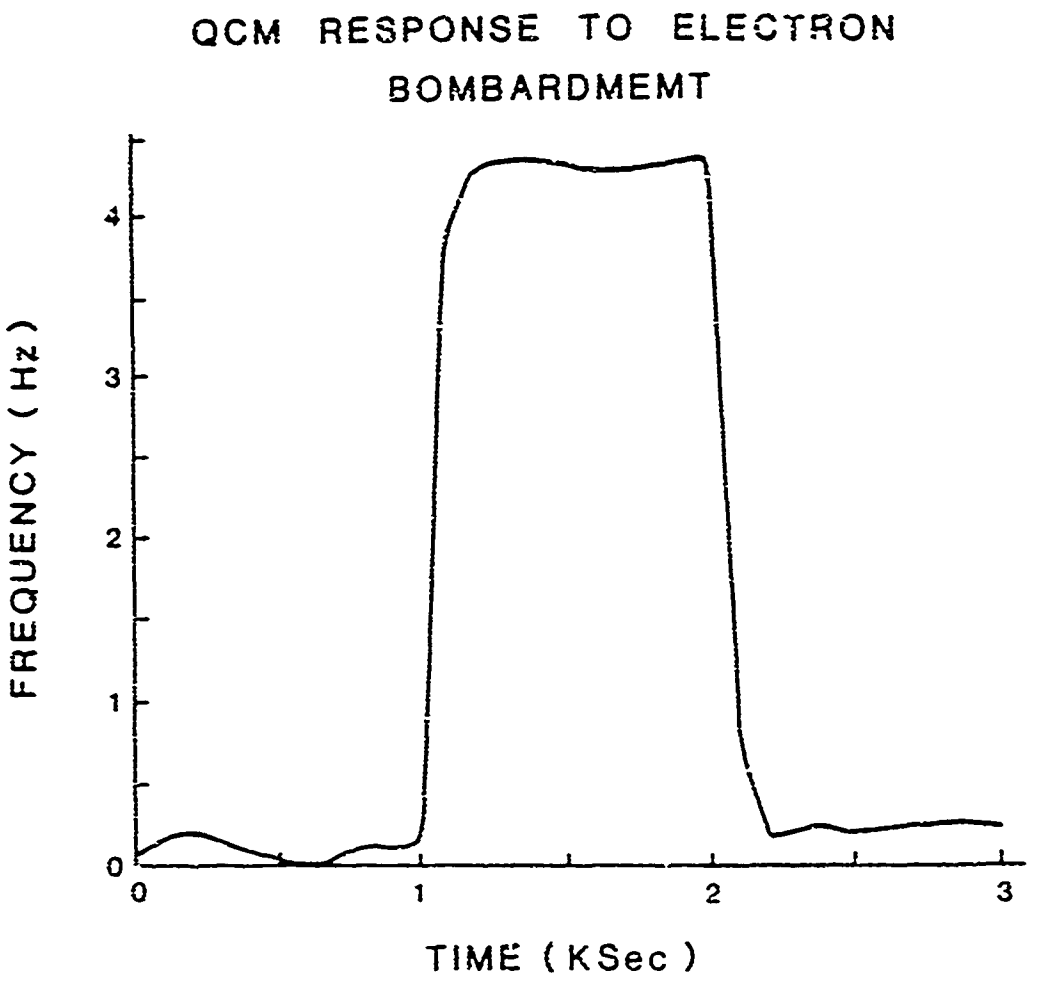

Fig. 5.4 QCM response to a 1 KeV, 1 uA electron beam incident on one face of the crystal.

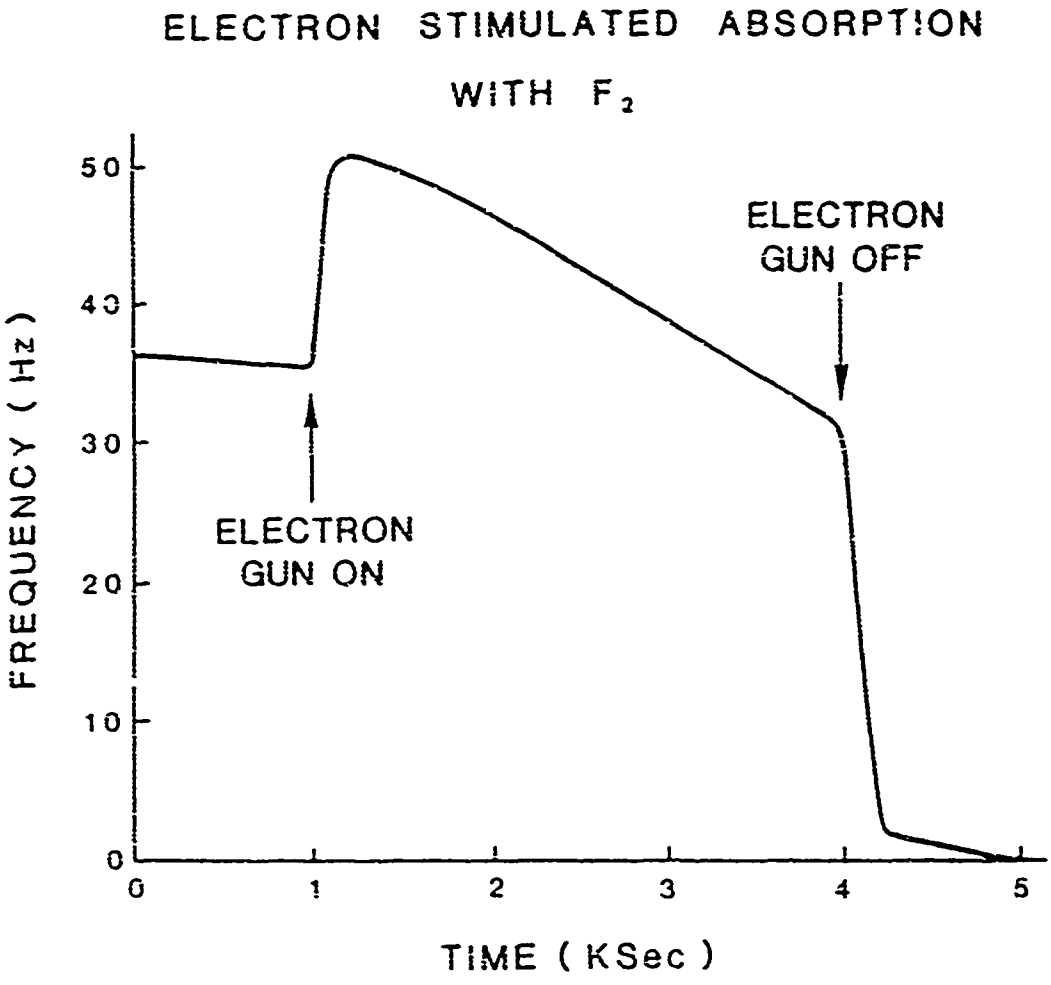

Fig. 5.5 QCM response during electron bombardment of silver in the presence of F_2.

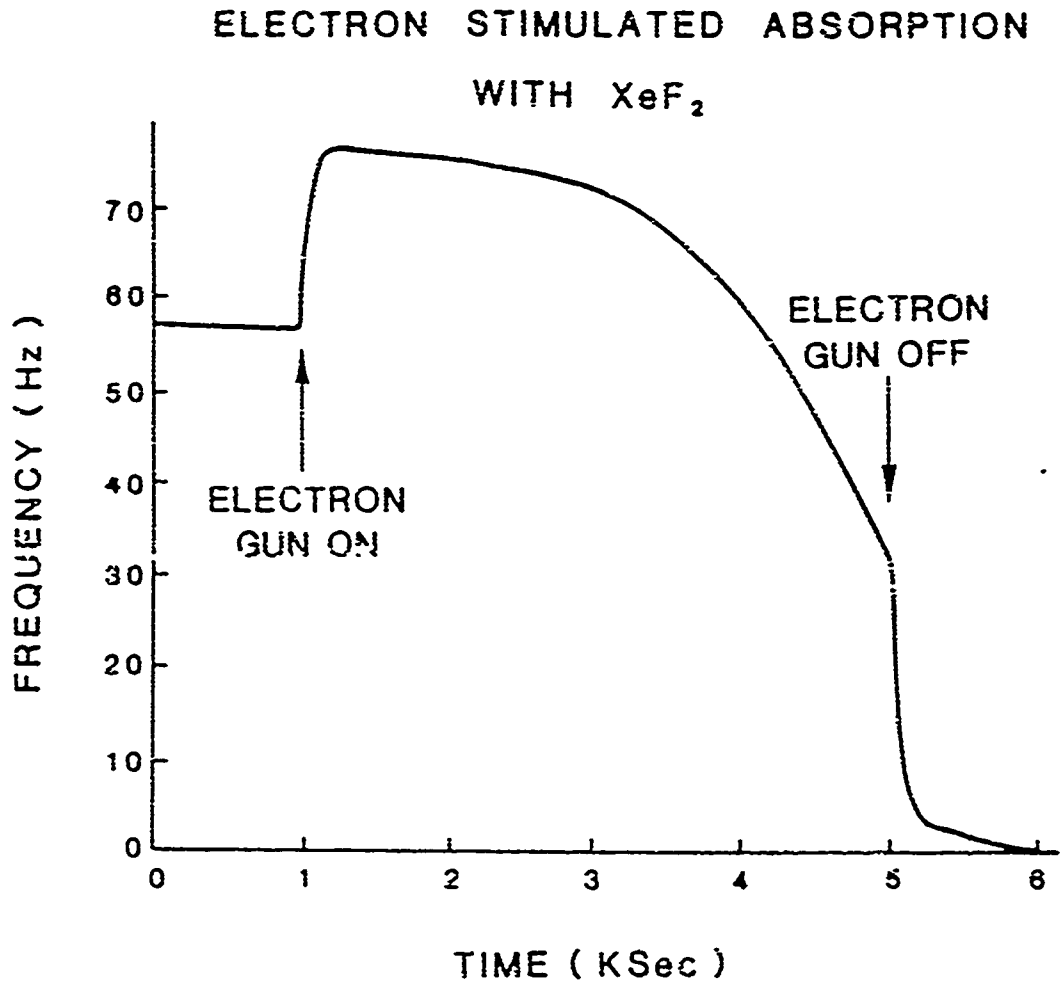

Fig. 5.6 QCM response during electron bombardment of silver in the presence of XeF_2.

uptake accelerated to a rate of 3.9 X 10^{-10} grams/s (9.3 X 10^{-3} monolayer/s) as the near surface fluorine concentration increased. This is an enhancement of 1.4 over the mass gain rate without the electrons present, and is a factor of 4 greater than the mass gain rate with F_2 and electrons.

The larger enhancement obtained with F_2 suggests that part of the enhancement mechanism involves the production of the more mobile and reactive species due to electron-induced dissociation. However, even with the XeF_2 exposed surface the electron bombardment increased the AgF growth rate. In the case of the XeF_2 exposed surface, the electron enhanced reaction rate may be due to a higher degree of dissociation and thus a higher concentration of the more mobile species on the surface. Other mechanisms that need to be considered include the creation of charged species whose mobility may depend on surface charging under electron bombardment and the excitation of activated systems to overcome energy barriers associated with chemical reactions and diffusion.

SILVER FLOURIDE GROWTH UNDER A THIN FILM

1000 A thin films of ThF_4, MgF_2, SiO_2, and Al_2O_3 deposited on a silver surface do not seem to present a significant barrier to fluorine uptake by the underlying

silver. Table 5.1 shows the rate of fluorine uptake on various thin film materials, deposited on a silver substrate, subjected to identical XeF_2 fluxes and a 1 KeV, 5 uA electron beam. A net mass gain was observed on a silver surface with an SiO_2 overlayer so long as the incident electron energy was below 200 eV. If the incident electron energy exceeded 200 eV etching occured and a net mass loss was observed, in agreement with Coburn and Winters' earlier findings (19). One important feature of these data is that silver surfaces overcoated with fluoride films gain mass at a faster rate than silver surfaces with oxide films or the bare silver surface itself. Note that the exposed silver electrodes surrounding the deposited film are on a relatively insensitive part of the crystal.

Fig. 5.7 shows the QCM response when a silver coated crystal with 1000 A of ThF_4 is simultaneously bombarded with by flux of XeF_2 and a 1 KeV, 5 uA electron beam. The large frequency rise observed when the electron gun is incident on the surface is due to two effects. First, there is the frequency rise due to the thermal gradient in the crystal created by electron bombardment as discussed in section 3.2. However, this should last for less than 300 s as opposed to the 600^+ s duration seen in Fig. 5.7. The prolonged rise in frequency is due to the electron stimulated decomposition of ThF_4 and desorption of the liberated fluorine (112). There is no accelerated mass

Table 5.1 Rate of fluorine uptake on a silver surface through various dielectric 1000 A thin films as determined by QCM.

thin film composition	electron energy (eV)	rate of mass gain (gram/s)	(monolayer/s)
ThF_4	1000	6.3×10^{-10}	1×10^{-2}
MgF_2	1000	5.9×10^{-10}	9.8×10^{-3}
Al_2O_3	1000	4.7×10^{-10}	7.8×10^{-3}
SiO_2	100	2.5×10^{-10}	4.2×10^{-3}
none (bare Ag)	1000	3.9×10^{-10}	6.6×10^{-3}

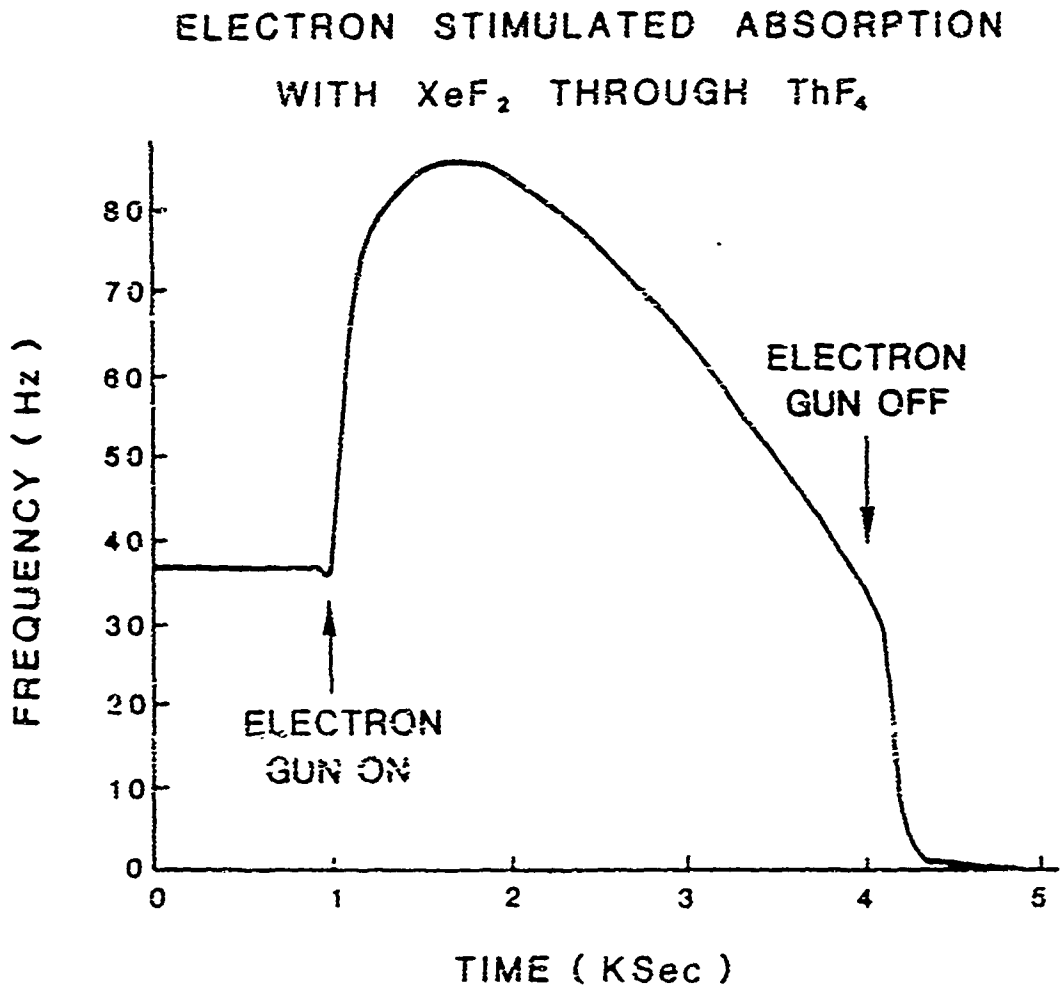

Fig. 5.7 QCM response during electron bombardment and XeF_2 exposure of a silver surface with a 1000 A ThF_4 film deposited on it.

gain rate with a ThF_4 film (Fig. 5.7) as there was in the case of no film (Fig. 5.6). We propose that the same fluorine species results from XeF_2 adsorption on a ThF_4 surface as is formed on an AgF surface and that this mobile species diffuses through the ThF_4 film until it reaches the silver where it reacts to form a silver fluoride layer. This is further substantiated by the fact that no net mass gain is seen when a ThF_4 film deposited on a gold substrate is subjected to identical conditions. Meakin (103) and Leamy et. al. (104) have demonstrated that such thin films may have an open, porous structure which may help to explain the ease with which this species seems to diffuse through them. The considerable ease with which fluorine diffuses through the ThF_4 along with the fluorine present in the ThF_4 itself results in a large fluorine concentration at the ThF_4 - silver interface. The large fluorine concentration that results may be equivalent to exposure of a silver surface to a larger flux of fluorine.

The rate of fluorine uptake on a bare silver surface stimulated by electron bombardment is largely unaffected by changes in the incident electron energy and depends linearly on the electron flux in the region investigated. The influence of the electron bombardment can be calculated by subtracting the mass gain rate before electron bombardment from that during electron bombardment to obtain the mass gain rate due purely to the electron enhancement.

This is then normalized by dividing by the electron current to obtain the enhanced fluorine uptake rate per electron (enhancement rate). This enhancement rate is plotted as a function of incident electron energy in Fig. 5.8. The enhancement rate on a bare silver surface (circles in Fig. 5.8) appears to be rather independent of the electron energy between 100 eV and 1 KeV. However, the enhancement rate on a silver surface with a 1000 A ThF_4 overlayer (crosses in Fig. 5.8) depends strongly on the incident electron energy. At energies greater than 300 eV the enhancement rate for the ThF_4 films is just slightly larger than that for bare silver. However, at energies below 200 eV the enhancement rate for the ThF_4 films is greater than that for bare silver by a factor of 5. Considering the penetration depth of the electrons this appears to be due to an increase in the electron enhanced fluorine sorption rate on the ThF_4 itself which may be caused by an increase in the fluorine surface to bulk diffusion cross section (112). Field enhanced processes may also play a role.

SUMMARY

In this section the electron enhanced growth of silver fluoride films on a silver surface in the presence of F_2 and XeF_2 was studied using AES, and QCM techniques. The fluorine uptake through various dielectric thin films

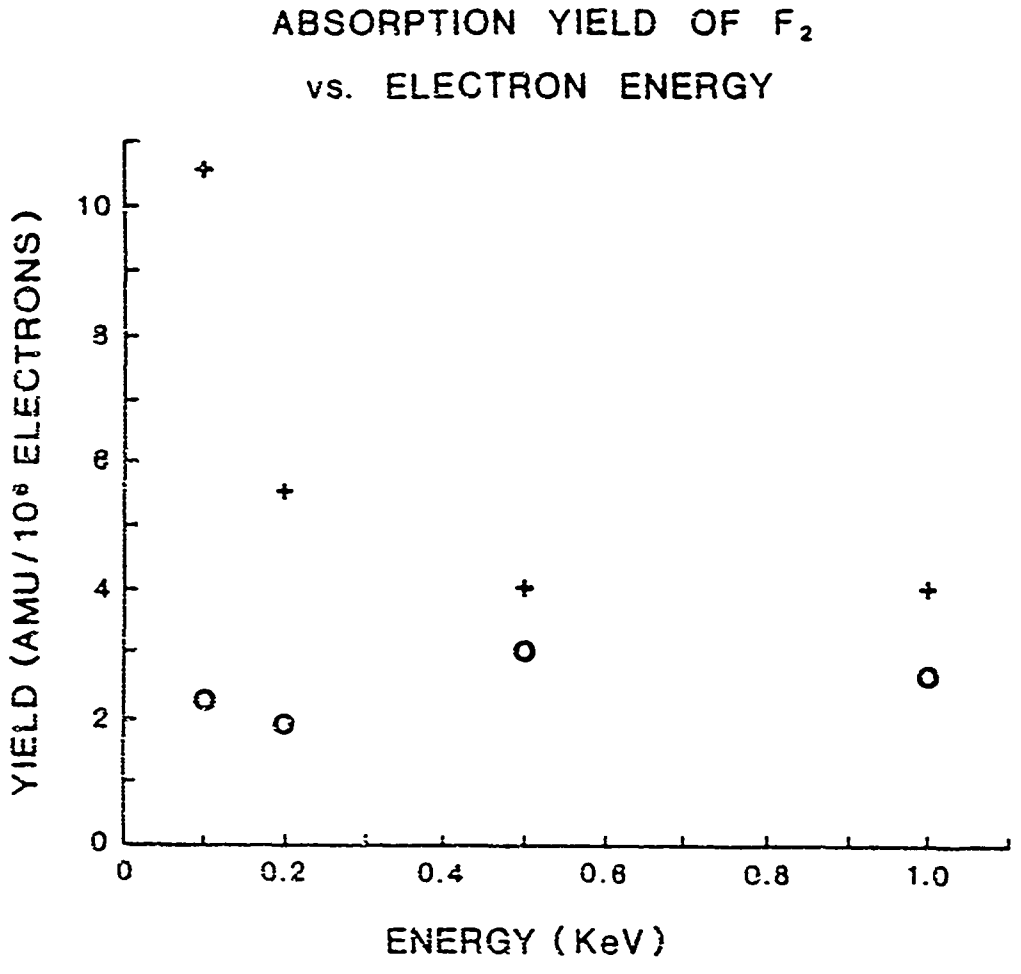

Fig. 5.8 Electron enhanced fluorine uptake rate per electron using F_2 and 5 μA electron beam. o = bare silver ; + = 1000 A ThF_4 film on silver.

was also investigated.

In the absence of electron bombardment, an initial layer (0.8 to 1.1 monolayer) of fluorine is adsorbed from F_2 and XeF_2 on a silver surface. This layer of fluorine slowly reacts with the silver and diffuses into the bulk of the silver at a rate of approximately 7×10^{-4} monolayer/s. As the near surface layers become fluorine enriched, an increasing amount of XeF_2 dissociatively chemisorbs which may result in a more mobile fluorine species thought to be atomic, which results in fluorine uptake at the faster rate of 6.5×10^{-3} monolayer/s.

When a flux of fluorine containing gas and a flux of energetic electrons were simultaneously incident on a silver surface, it was discovered that the fluorine uptake rate on a silver surface exposed to F_2 increases by a factor of 3 to 2.3×10^{-3} monolayer/s. The rate of Fluorine uptake on a silver surface exposed to XeF_2 increased by a factor of 1.4 to 9.3×10^{-3} monolayer/s. This may be the result of the formation of additional mobile fluorine from the F_2 or XeF_2 adsorbate by the electrons. The electron enhanced fluorine uptake rate does not strongly depend on the incident electron energy in the 100 eV to 1 KeV energy range.

When a thin film coated on a silver substrate was simultaneously exposed to a flux of XeF_2 and a flux of electrons it was discovered that electron-enhanced fluorine

uptake into the silver substrate occurs through a variety of thin film materials (ThF_4, MgF_2, SiO_2, and Al_2O_3). Electron enhanced fluorine uptake appears to be faster through fluoride films than through oxide films or on a bare silver surface. XeF_2 appears to dissociatively chemisorb on ThF_4 resulting in a mobile fluorine species which can easily diffuse through the ThF_4 to the silver where it may form an AgF layer.

VI. ELECTRON INDUCED DAMAGE OF ThF_4 THIN FILMS IN THE PRESENCE OF XeF_2

During Ar ion sputtering, AES revealed traces of carbon and oxygen in the bulk of the ThF_4 films, almost at the same concentration as on the surface initially. The presence of oxygen in ThF_4 usually indicates water (105). Exposure of the surface to XeF_2 rapidly removes most of the surface impurities, especially during electron bombardment, although one must keep these trace impurities in mind when evaluating the results.

EFFECT OF ELECTRON BOMBARDMENT ON ThF_4

ThF_4 rapidly loses mass during electron bombardment, as indicated by microbalance measurements. The microbalance measures total mass loss which includes the mass of + or - ions and neutral particles. Simultaneous with this mass loss, the quadrupole mass spectrometer registered a substantial (up to 28%) increase in the 38 AMU (F_2) peak. Since the quadrupole is not in line of sight with the ThF_4 it is unlikely that it would detect atomic fluorine due to wall collisions. Although no increase in the 19 AMU (F_2) peak was measured, there is a strong possibility that at least part of the desorbing fluorine is atomic.

The atomic concentration of surface species was monitored with AES during an extensive exposure to 1 keV electrons and is plotted in Fig. 6.1. The fluorine concentration decreases from 75% to 50% during the first 0.01 C (3 X 10^{17} electrons/cm^2) of bombardment, with little change in fluorine concentration thereafter. The thorium concentration initially increases due to the loss of fluorine and then decreases as the film slowly adsorbs carbon and oxygen containing gases from the background. The sticking probability of the residual gas on the ThF_4 surface is increased by the removal of fluorine.

The damage caused by electron bombardment is not limited to the near surface layers. Microbalance measurements indicate that during extensive bombardment with a 1 keV, 50 uA electron beam, the fluorine loss is equivalent to all the fluorine contained in up to 27 monolayers of ThF_4. The damage actually extends much deeper than 27 monolayers since AES indicates that surface fluorine still remains after bombardment. This bulk damage is accompanied by a visible change in the ThF_4 film. The film develops a dark blue color where the electron beam was incident upon it. This blue color is due to bulk defects or color centers which presumably are associated with fluorine vacancies. No information on ThF_4 color centers could be found in the literature. This blue color is

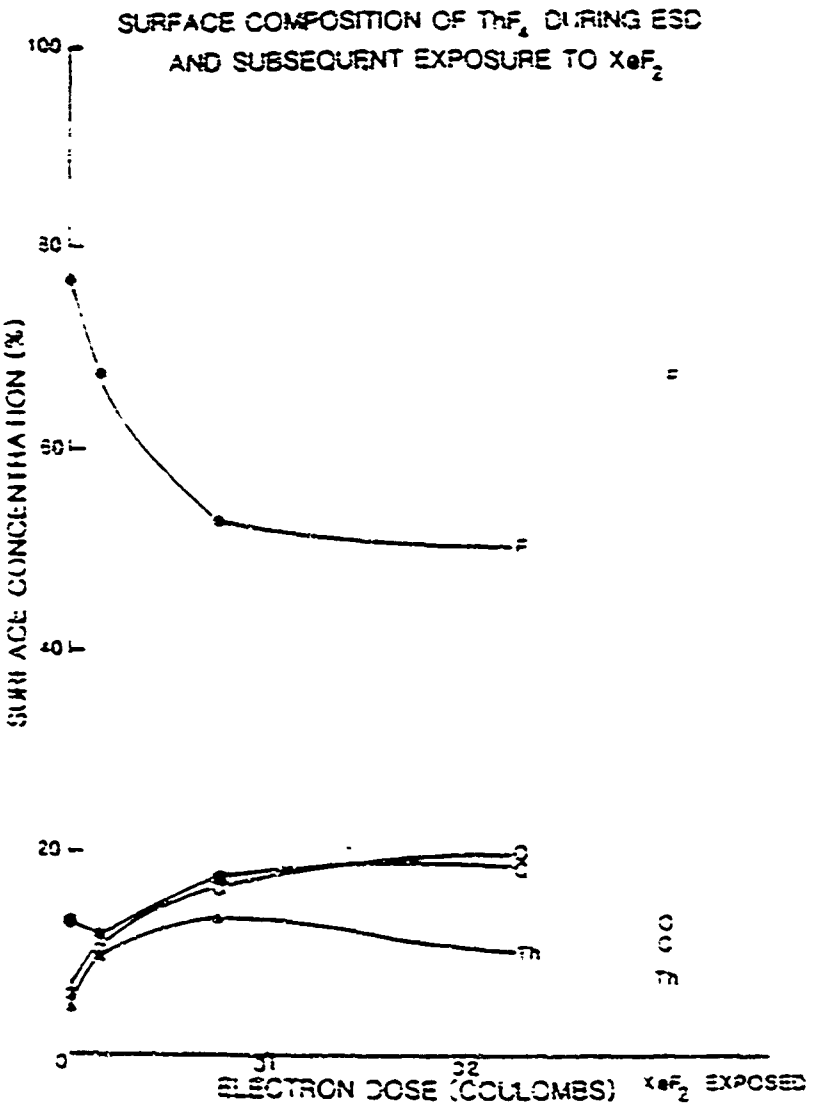

Fig. 6.1 Concentration of fluorine, oxygen, carbon, and thorium on the surface as determined by AES during Electron Stimulated Desorption of ThF_4 with 1 keV electrons. Symbols on far right represent surface concentrations after electron bombardment is halted and the sample is exposed to XeF_2.

visibly diminished after the film reabsorbs a large amount of fluorine.

For a ThF_4 film to lose many monolayers of fluorine very quickly under electron bombardment in a vacuum, electron bombardment must stimulate the following processes: ThF_4 dissociation, fluorine bulk diffusion in the near surface layers, bulk to surface diffusion (surface segregation), and fluorine desorption. Without electron bombardment, fluorine would not be driven to the surface very quickly by the concentration gradient. Indeed, under certain circumstances, ThF_4 can rapidly gain many monolayers of fluorine assisted by electron stimulated diffusion.

The initial rate of mass loss of ThF_4 subjected to electron bombardment at various energies from 50 eV to 500 eV was measured. Fig. 6.2 shows the dependence on electron energy of the yield (mass loss rate/electron flux) during the first 100 s of ESD with a low intensity beam of electrons. The electrons are very efficient at desorbing fluorine; almost every electron removes a fluorine particle. The sudden jump in yield between 200 and 250 eV is readily apparent, and we suggest that it is due to a Knotek-Feibelman desorption mechanism (9-10). The incident electron would cause ionization of a thorium-O shell (229 eV), followed by an intra-atomic Auger decay leaving the fluorine positively charged. The fluorine should then

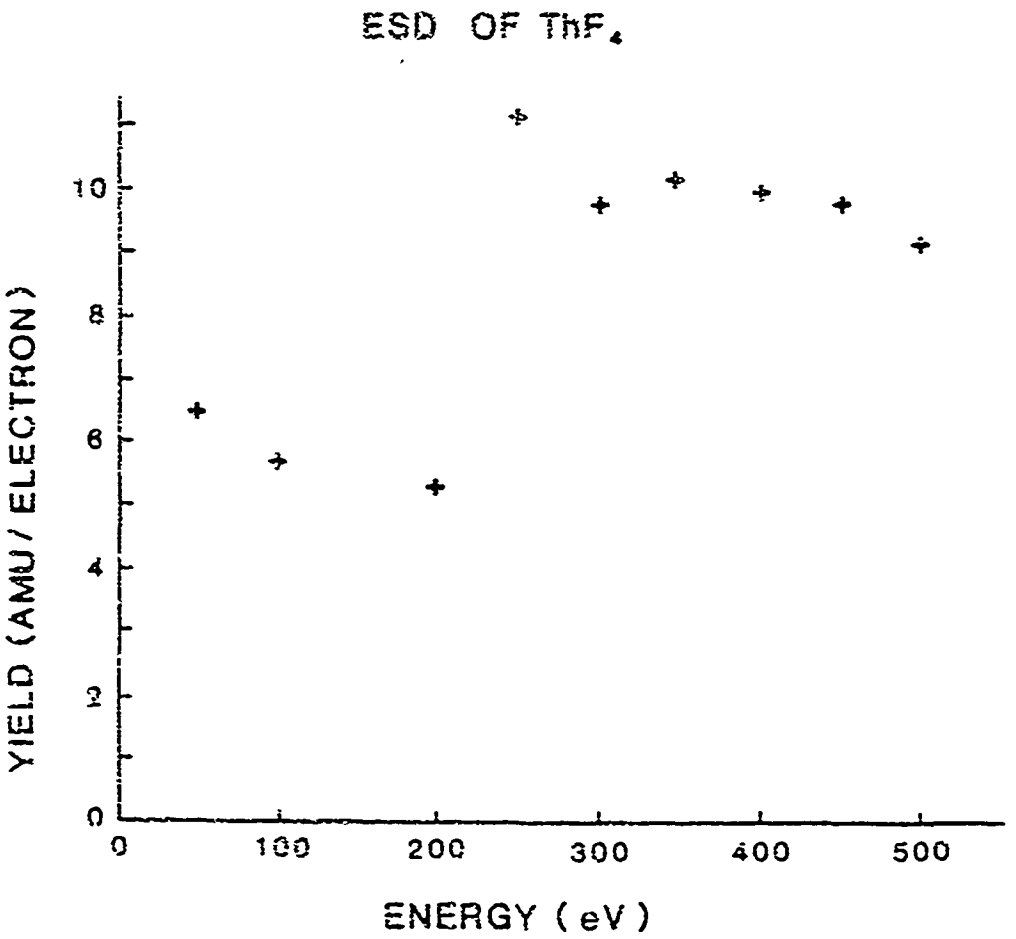

Fig. 6.2 Electron energy dependence of Electron Stimulated Desorption of fluorine from ThF_4 as determined by QCM.

desorb as F^+ or neutral F. This requires further experimental verification with line of sight mass spectroscopy.

EXPOSURE OF ELECTRON DAMAGED ThF_4 TO XeF_2

When "virgin" ThF_4 is exposed to XeF_2 it slowly adsorbs a fraction of a monolayer of fluorine (typically 0.7 monolayer). The sticking probability is small and can vary considerably from one sample to the next due to surface contamination. Xenon could not be detected with AES. The surface fluorine concentration was seen to rise by only about 5%, indicating that some of the fluorine may have diffused into the bulk.

We have found that a fluorine depleted ThF_4 film (such as that at the completion of electron bombardment in Fig. 6.1) readily adsorbs fluorine. When such a surface is exposed to XeF_2, it rapidly gains a monolayer of fluorine with unity sticking probability. After 1 monolayer is adsorbed, the fluorine adsorption continues at a very slow rate with less than an additional monolayer adsorbed after several hours. The data at the right side of Fig. 6.1 shows the increase in surface fluorine concentration which occurred after electron bombardment was halted and the sample was exposed to XeF_2.

SIMULTANEOUS EXPOSURE TO ELECTRONS AND XeF_2

When a ThF_4 surface is simultaneously exposed to XeF_2 and 1 keV electrons, it loses less total fluorine than it would if the XeF_2 were not present. Under the identical 1 keV electron beam used before, the maximum fluorine a ThF_4 film would lose, when subjected to a flux of XeF_2, was 13 equivalent monolayers or about half of what it would lose in vacuum. Fig. 6.3 shows the concentration of surface species as determined by AES during simultaneous exposure to XeF_2 and a 1 keV electron beam. Note the rapid initial loss of carbon which causes the thorium concentration to increase. The fluorine concentration on the surface increases to 80% at a total electron dose of 0.008 C, then slowly decreases.

ESD of ThF_4 must still be occurring under these circumstances. However, an empty surface site is quickly filled from the gas phase. The diffusion of the near surface fluorine is still stimulated by electron bombardment and this results in a fluorine enriched surface. After some time, however, the bulk fluorine concentration decreases until a chemical equilibrium is established where fluorine is desorbed from the surface at the same rate as it is adsorbed from the gas phase.

At low incident electron energies (below 150 eV), this chemical equilibrium is not established for very long

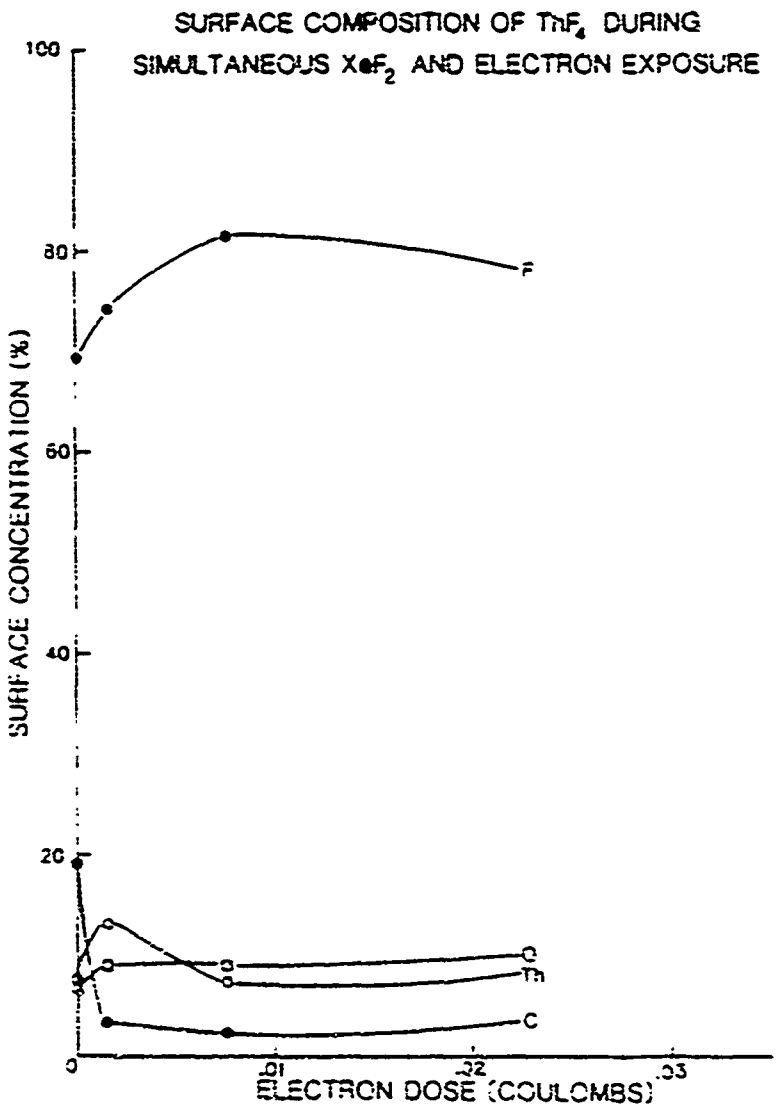

Fig. 6.3 Surface concentration of fluorine, oxygen, carbon, and thorium as determined by AES during simultaneous exposure to 1 keV electrons and 3.5×10^{15} XeF_2 molecules/cm^2/s.

periods of time. During simultaneous bombardment with low energy electrons and XeF_2, the ThF_4 film gains mass at a steady rate depending on electron energy, XeF_2 flux, and electron flux. After 2 hours of bombardment with 7 uA, 100 eV electrons and 1 X 10^{16} XeF_2 molecules/s, the mass gain rate showed no change. From our microbalance measurements, we can calculate a "sorption yield" which is equal to the rate of mass gain/electron. Fig. 6.4 shows the dependence of the sorption yield on incident electron energy measured by the microbalance during bombardment with 1 uA of electrons. The mass gain rate appears to peak at 50 eV, suggesting that this is the energy at which the diffusion of fluorine from the surface into the bulk is maximized. If at this energy the cross section for fluorine segregation into the bulk is a maximum, then the fluorine flow would be regulated at the surface by the incoming gas phase fluorine (XeF_2) and the electron current and not by the bulk concentration gradient. Field stimulated effects may also play a role since the secondary electron yield decreases at these low energies, resulting in increased surface charging.

Large fluorine concentrations can be pumped into a ThF_4 thin film. Fig. 6.5 shows the XeF_2 flux dependence of the sorption/ESD yield as measured by the microbalance. With 1 keV (circles in Fig. 6.5; incident electrons, ESD dominates until an XeF_2 flux of 4 X 10^{15} molecules/s is

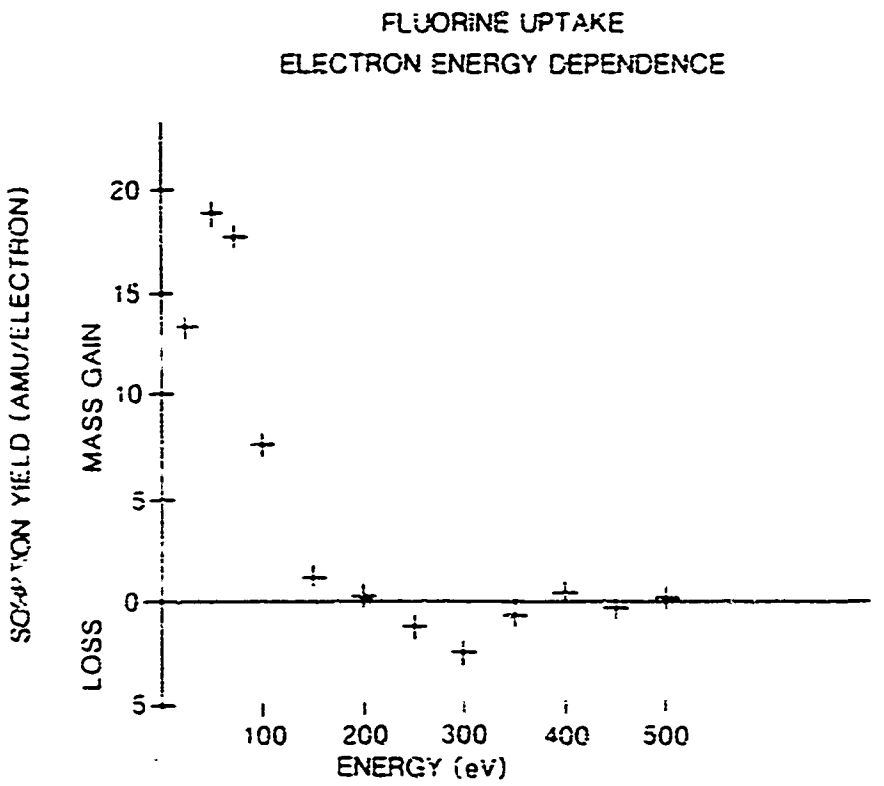

Fig. 6.4 Yield (mass change/electron current) dependence on electron energy during simultaneous exposure to XeF_2 and electrons.

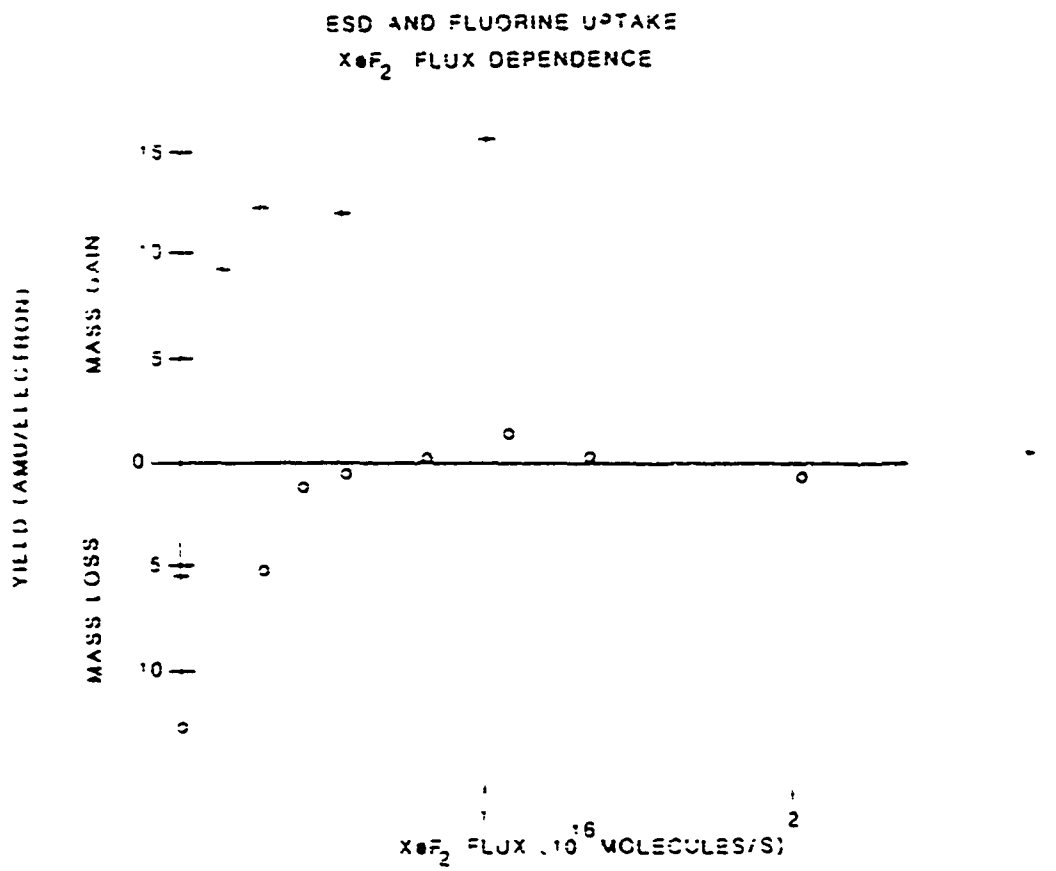

Fig. 6.5 Dependence of the sorption-ESD yield of ThF_4 film on XeF_2 flux during electron bombardment with 1 keV (circles) and 100 eV (crosses) electrons.

reached, which is when chemical equilibrium is rapidly established. When 100 eV (crosses in Fig. 6.5) electrons are incident, a very small flux of XeF_2 (less than 3.5×10^{14} molecules/s/cm^2) is required for significant sorption to take place.

In Fig. 6.6, we show the electron flux dependence on the mass change of a ThF_4 film exposed to 3.5×10^{15} XeF_2 molecules/s/cm^2 and electrons. For 1 keV electrons (circles in Fig. 6.6), ESD is more dominant at large electron fluxes (10 uA), as one would expect. With 100 eV electrons incident (crosses in Fig. 6.6) and at low fluxes, the reaction is electron current limited. The fluorine which segregates from the surface to the bulk is regulated by the electron flux. At higher current, the reaction becomes gas flux limited starting at 4 uA when the rate of fluorine segregation into the bulk is limited by the gas phase fluorine reaching the surface. At higher electron fluxes, the sorption yield decreases because ESD is occurring faster than adsorption from the gas phase. The surface fluorine concentration is reduced and therefore segregation into the bulk is slightly slower.

It should be noted that the results obtained with F_2 as a gas phase fluorine source were almost identical with those obtained with XeF_2 when care was taken to carefully match the fluxes for the two gases.

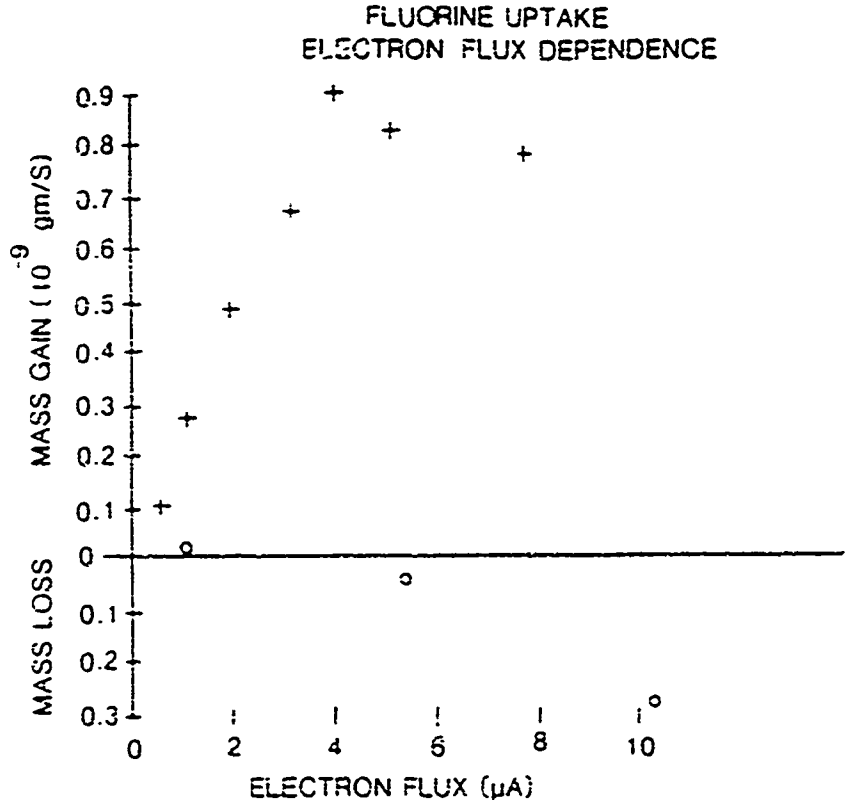

Fig. 6.6 Electron flux dependence of the mass change of a ThF_4 film while exposed to XeF_2 for electron energies of 1 keV (circles) and 100 eV (crosses).

VII. CHEMISORPTIVE EMISSION FROM FLUORINE ADSORPTION ON TUNGSTEN

RESULTS

Tungsten was observed to emit electrons during exposure to F_2. Prior to cleaning no CE was observed from the filament. Immediately after flashing, a small electron count rate was measured as seen at the beginning of Fig. 7.1 due to background F_2. Gas exposure occurred approximately 2 s after flashing when the temperature of the tungsten was 588 K. The rate of electron emission changes dramatically with time and begins immediately with the onset of gas exposure, as seen in Fig. 7.1 (crosses correspond to electron emission rate and circles correspond to gas flux). The rising edge of the emission peak is due to the rising gas flux. As the surface coverage increases the count rate decreases to zero.

The total number of electrons counted, i.e., the area under the emission curves, remains constant for a wide variety of F_2 pressure profiles at fixed temperature. Three such CE curves are shown in Fig. 7.2 (crosses represent data) for F_2 adsorption on tungsten for different maximum F_2 fluxes. Fig. 7.2a corresponds to the largest maximum F_2 flux and Fig. 7.2c to the lowest. The CE peaks

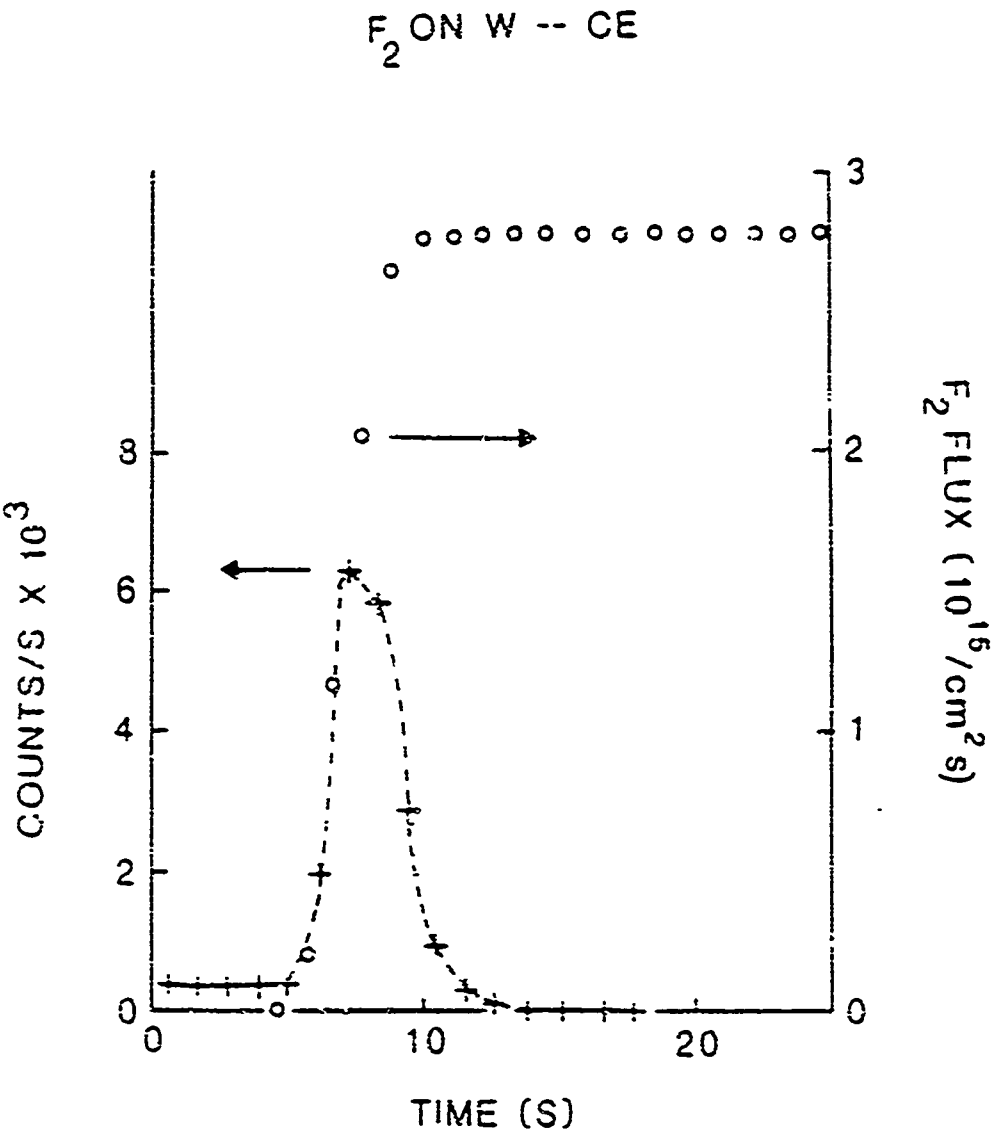

Fig. 7.1 CE rate of clean tungsten exposed to F_2. Electron emission rates are represented as crosses. The gas flux is represented as circles.

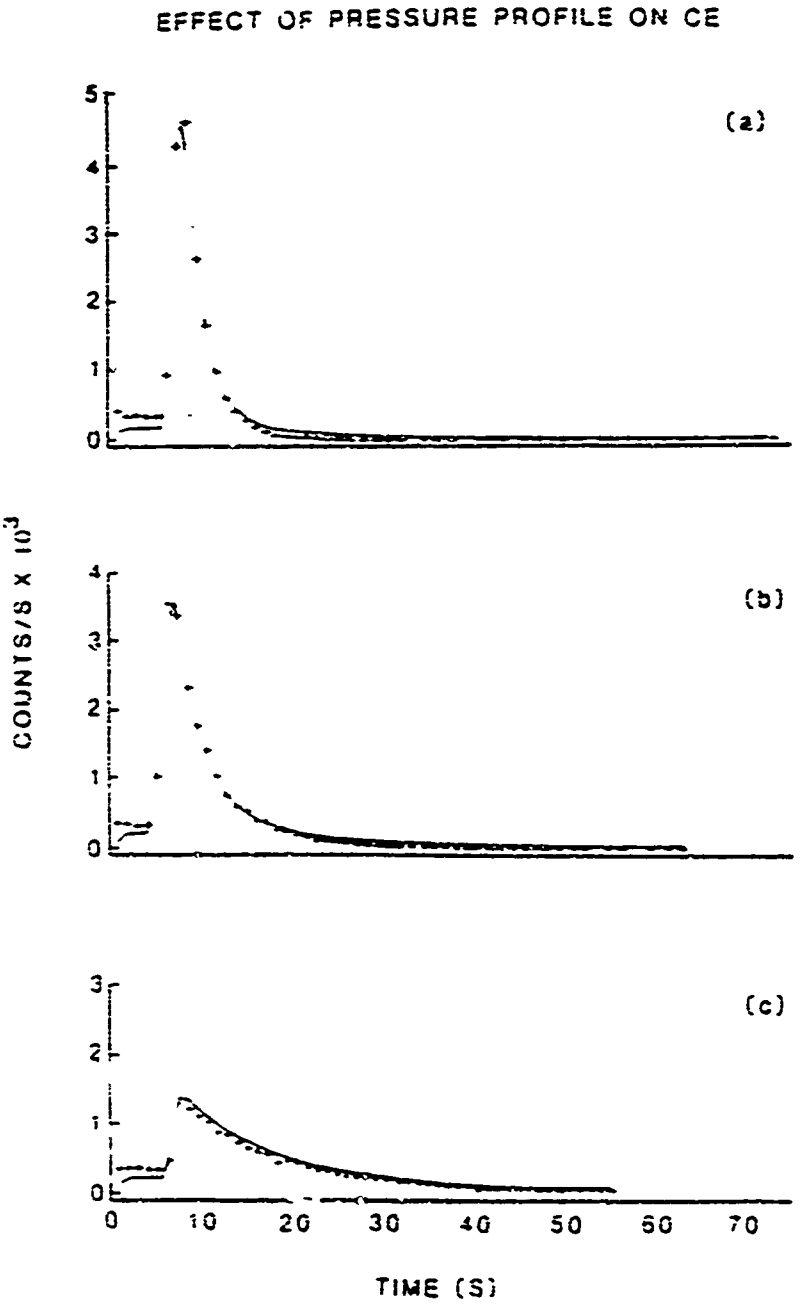

Fig. 7.2 CE rate during 3 successive exposures of clean tungsten with different F_2 flux profiles. (a) large flux (b) medium flux (c) low flux. The lines represents the fit predicted by the model.

corresponding to smaller maximum F_2 fluxes have a smaller maximum value but last longer in time; the total number of counts (area under the curve) remains unchanged.

At higher filament temperatures, the maximum count rate as well as the total number of counts increases. Fig. 7.3a displays the data (crosses) for the highest tungsten temperature and Fig. 7.3c for the lowest. Care was taken to stay below the temperature at which thermionic emission from the tungsten interfered. Thermionic emission was measurable at 1140 K and 1230 K for a clean tungsten surface and a fluorine covered tungsten surface, respectively. The temperature dependence of the total number of counts, during the exposure of a clean tungsten surface to F_2, is plotted in Fig. 7.4 (crosses). The temperature dependence appears to be exponential. The data point at 1141 K may have a small contribution due to thermionic emission. No evidence of steady state CE due to spontaneous etching of W by F_2 was observed. We believe that this is due to the increase in work function by the electronegative adsorbed fluorine.

Although a small CE peak was observed when a clean tungsten sample was exposed to XeF_2, it was found that once the XeF_2 flux was purged of impurities (e.g. O_2, CO, H_2O, and F_2) the count rates dropped considerably. AES, however, reveals that XeF_2 <u>does</u> dissociatively chemisorb on W, resulting in a layer of fluorine of the same coverage as

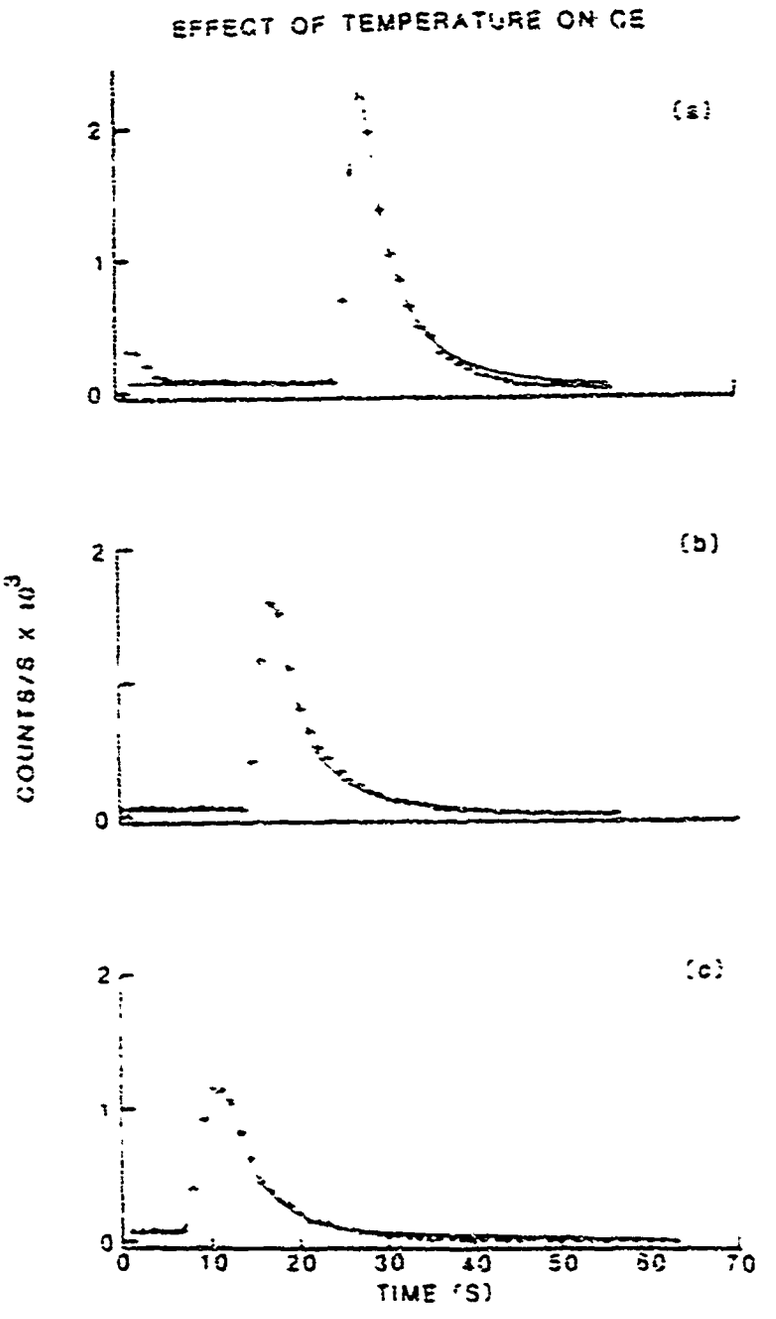

Fig. 7.3 CE rate during 3 successive exposures of clean W to F_2 for different tungsten temperatures: (a) 776°K (b) 669°K (c) 588°K. The lines represent the fit predicted by the model.

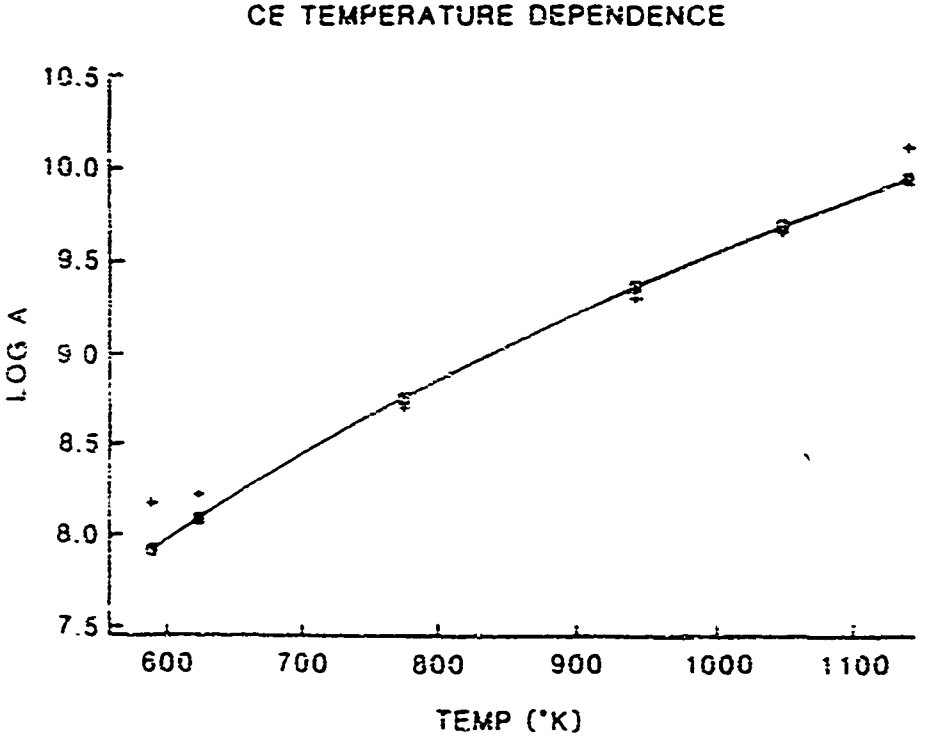

Fig. 7.4 Temperature dependence of the total number of electrons detected from W surface during F_2 exposure plotted on a log scale (crosses). The squares represent the best fit predicted by the model.

that produced by exposure to F_2. We conclude that the CE measured during XeF_2 exposure is due to the adsorption of background gases (including F_2) and that a very small amount or no CE occurs when XeF_2 is adsorbed on W.

DISCUSSION

In the Norskov-Kasemo model (30,33), the excited state results from the rapid approach of the molecule to the surface. If the molecule is approaching the surface slowly, the hole may be filled from the surface as that energy level shifts below the Fermi level (an adiabatic transition), thus an energetic electron transition does not occur as the molecule approaches the surface. The component of the average velocity normal to the surface, of an XeF_2 molecule is a factor of 0.05 smaller than that of an F_2 molecule due to the large mass difference. This may account for the lack of CE observed during XeF_2 adsorption because adiabatic transitions are more likely. In addition to the mass difference, the presence of the electronic structure of the xenon may also play a role in preventing the formation of a low lying hole in the adsorbed atom.

To probe the relation of CE to chemisorption, we explored a kinetic model for CE from the exposure of tungsten to F_2. We assumed that the rate of electron emission, R, is proportional to the rate at which surface

sites are being filled, where θ represents the fractional fluorine coverage; i.e.,

$$7.1 \qquad R = -K(\theta)\, d\theta/dt$$

We expect a coverage dependent rate constant due to an increase in the work function with increasing θ.

The rate at which sites are being filled is assumed to be proportional to the number of sites which are not filled (i.e. first order adsorption):

$$7.2 \qquad -d\theta/dt = F(t)S(\theta)N_o(1-\theta)$$

Here F(t) represents the time dependent gas flux, S(θ) the sticking probability, and N_o the total number of sites (calculated to be 10^{14}). The rate of electron emission can be written as a function of coverage:

$$7.3 \qquad R = FK'G(\theta)(1-\theta)$$

The θ dependence of the sticking probability, as well as the probability for electron emission per site is contained in the function G(θ).

During our experiments, the gas flux $F(t_i)$ and the number of emitted electrons $C(t_i)$ occurring during the time interval from t_i to $t_i+\Delta t$ were measured, where the

coverage increases from 0 at t=0 to 1 at t= ∞ .

$$7.4 \qquad C(t_i) = \int_{t_i}^{t_i + \Delta t} R(t)dt$$

Equations 7.3 and 7.4 were numerically solved using standard integration techniques and the measured R(t). K' and simple functions for G(θ) were adjusted to minimize the sum of the squares of the deviations between predicted values from equation 7.4 and the experimental data. A simple G(θ) function, given by equation 7.5, with the single adjustable parameter r was found to yield agreement between equation 7.3 and the data. θ_{max} is the coverage at which the emission goes to zero.

$$7.5 \qquad G(\theta) = \begin{cases} 1 & \text{for } \theta \leq r\theta_{max} \\ \sqrt{\dfrac{1 - \theta/\theta_{max}}{1 - r}} & r\theta_{max} < \theta < \theta_{max} \end{cases}$$

This function G(θ), plotted in Fig. 7.5, decreases to zero as θ increases. This is a reasonable form for the product of a typical sticking probability and a function of θ representing the effect of an increasing work function. An increasing work function, due to the increasing

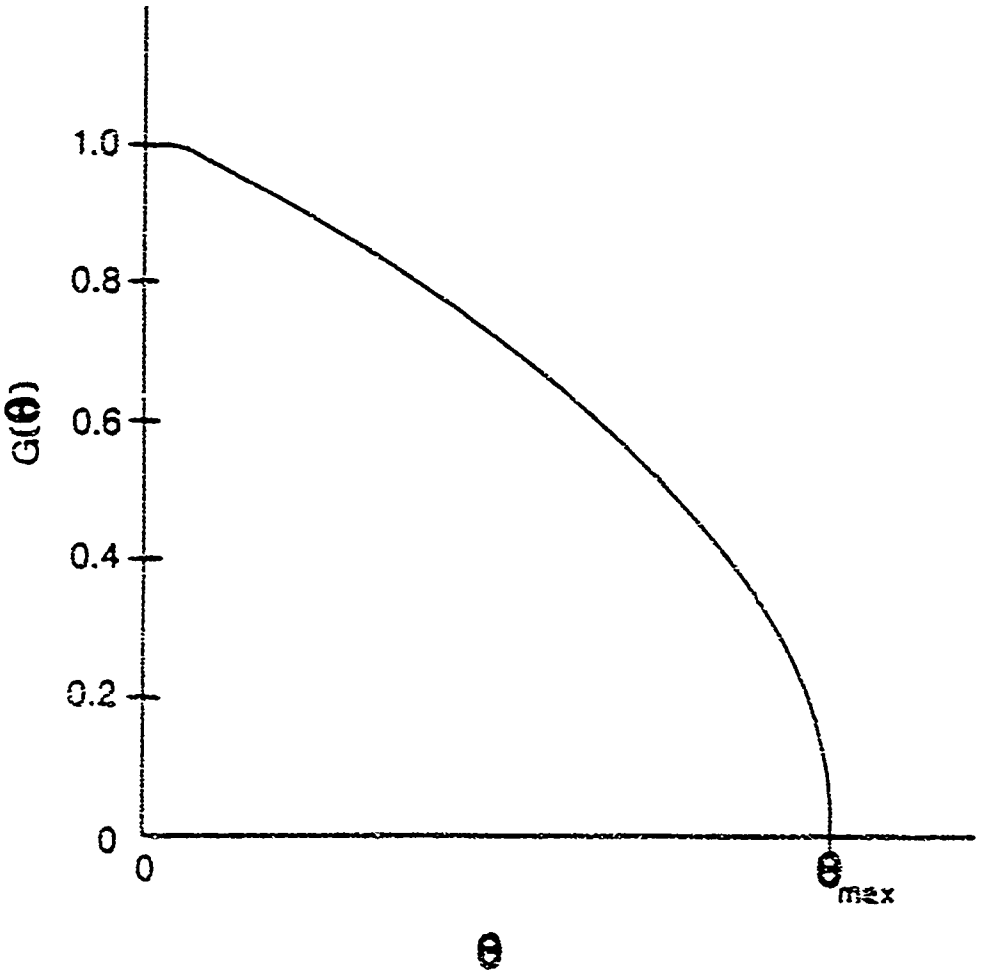

Fig. 7.5 Coverage dependent function used to model CE.

concentration of electronegative fluorine on the surface, results in a decreasing probability for an electron escaping. We suspect that for $\theta = \theta_{max}$ this probability is vanishingly small because at high F_2 fluxes the CE curves following their peaks drop to zero emission so decisively even though an etching reaction is probably occurring which would free new W adsorption sites (but at high θ).

This model, with the same values of r and K', fits quite nicely the CE data taken with different gas flux profiles, as seen in Fig. 7.2. Here the crosses represent actual data and the lines represent the predicted behavior using the measured F(t). The model fits the data at all gas flux vs. time profiles that we examined. The poorest fit occurred with low F_2 fluxes (Fig. 7.2c), most likely due to the larger role played by the background gases when the F_2 flux is relatively low.

This same model was also used to fit CE data taken at different temperatures, as shown in Fig. 7.3. Again crosses represent the actual data and the lines are the predicted emission curves using the measured F(t). It was only necessary to change K' to fit the data at different temperatures i.e., r was held constant. This implies that the temperature dependence is exclusively contained in the factor K'(T), decoupled from the coverage dependence and that the sticking probability function is unaffected by T over the range studied.

The average probability per site for electron emission at a given temperature can be calculated by dividing the total number of electrons emitted at that temperature by the number of sites on the surface. At 588 K, the lowest temperature, 10^4 electrons are typically emitted. The average probability for electron emission per site is therefore 10^{-10}. In Fig. 7.4 we show on a log intensity scale the increase in the emission probability per site with temperature. We propose that this is due to the increasing number of electrons occupying energies above the Fermi level of the metal, E_f, at higher temperature.

To model this temperature dependence, we assume an electron with energy E_1, in the tungsten (Fig. 7.6), fills the hole in the adsorbed fluorine electronic structure E_a. The energy from this process is imparted to a second electron in the tungsten conduction band which originally had energy E_2. If the energy of the second electron is greater than E_v, the vacuum level (relative to the bottom of the conduction band), the electron may leave the surface, i. e. if $E_2 + E_1 - E_a > E_v$, illustrating why an increasing work function could cut off the CE. This yields a condition on the energy of the second electron (E_2) for emission to occur:

$$E_2 > E_v + E_a - E_1 \qquad 7.6$$

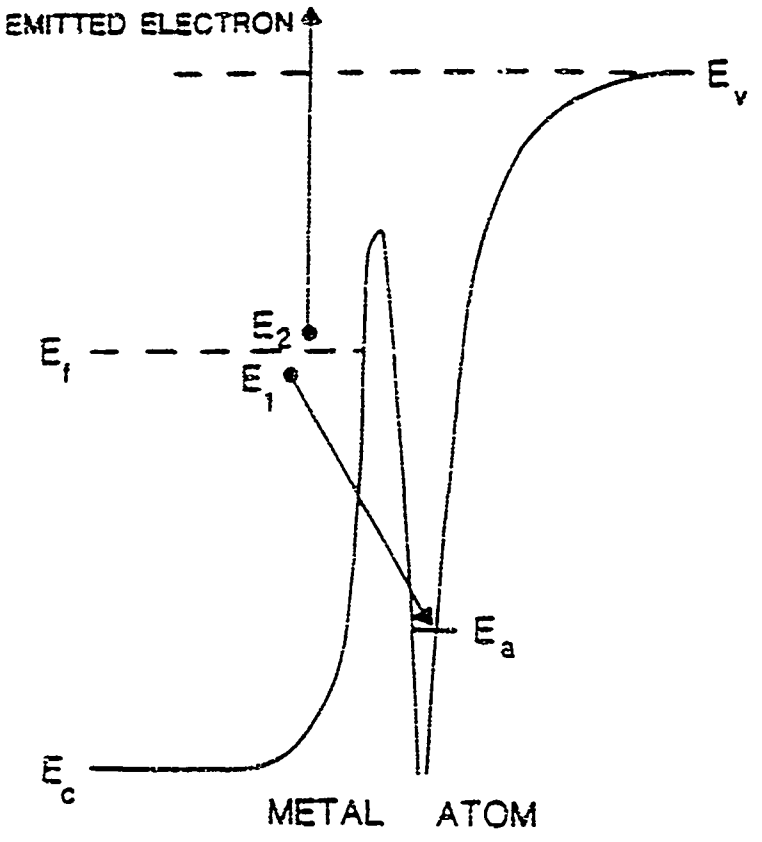

Fig. 7.6 Energy level diagram of the 2 electron process resulting in CE; E_c = bottom of the conduction band, E_a = energy level of the electron hole in the fluorine electronic structure, E_f = Fermi energy, E_v = vacuum energy level, E_1 = original energy of the electron that fills the hole in the fluorine electronic structure, E_2 = original energy of the emitted electron.

The density of occupied electron energy states in tungsten can be approximated by a $(\text{energy})^{1/2}$ dependence, measured from the bottom of the conduction band (106-108). Using a Fermi-Dirac electron occupation distribution we arrive at the electron energy distribution in Eq. 7.7. We take for these calculations a Fermi energy of 9 eV from the bottom of the conduction band (106).

$$7.7 \qquad n(E) = \frac{\sqrt{E}}{\exp((E-E_f)/kT)+1}$$

Integrating over the energy of both electrons (E_1 and E_2) involved in the emission process, the total emission vs. temperature is given by:

$$7.8 \qquad A = L \int_{E_a}^{\infty} \frac{\sqrt{E_1}\ dE_1}{\exp((E_1-E_f)/kT)+1} \int_{E_v+E_a-E_1}^{\infty} \frac{\sqrt{E_2}\ dE_2}{\exp((E_2-E_f)/kT)+1}$$

where L is simply a scaling factor and E_a is considered to be an adjustable parameter. Eq. 7.8 thus represents the temperature dependence of our model. An effective work function $(E_v - E_f)$ of 4.5 eV for tungsten was used (109).

Using a non-linear least squares curve fitting program, L and E_a were adjusted to obtain the best fit to

the experimental values in Fig. 7.4; the predicted values are shown as squares. Considering its simplicity this model fits reasonably well. We attribute, at least in part, the deviation at high temperature to thermionic emission. The effective energy level of the fluorine hole (E_a) which provided the best fit was found to be 4.45 eV below the Fermi level. The energy obtained by filling this level with an electron at the Fermi level is not sufficient to cause the emission of a second electron at the Fermi level. Therefore this process involves at least one electron above the Fermi level. Since the number of electrons above the Fermi level at the temperatures studied here is small, this may account for the small emission probability per site observed.

ACKNOWLEDGEMENTS

The authors wish to thank Dr. Ansgar Schmid, Laboratory for Laser Energetics, University of Rochester, for his participation in the work reported here. We also thank Dr. William G. Durrer for his assistance in preparing this report.

REFERENCES

1. J. W. Coburn, Plasma Etching and Reactive Ion Etching (AVS Monograph Series 1982).
2. D. L. Flamm, V. M. Donnelly, and D. E. Ibbotson, J. Vac. Sci. Tech. B 1 (1983) 23.
3. E. A. Knabbe, J. W. Coburn, and E. Kay, Surf. Sci. 123 (1982) 427.
4. D. L. Flamm, D. E. Ibbotson, J. A. Mucha, and V. M. Donnelly, Solid State Tech. 26 (1983) 117.
5. U. Gerlach-Meyer, Surf. Sci. 103 (1981) 524.
6. U. Gerlach-Meyer, J. W. Coburn, and E. Kay, Surf. Sci. 103 (1981) 177.
7. H. F. Winters, J. W. Coburn, and T. J. Chuang, J. Vac. Sci. Tech. B 1 (1983) 469.
8. Y. Tu, T. J. Chuang, and H. F. Winters, Phys. Rev. B 23 (1981) 823.
9. T. M. Mayer, R. A. Barker, and L. J. Whitman, J. Vac. Sci. Tech. 18 (1981) 340.
10. R. A. Barker, T. M. Mayer, and W. C. Pearson, J. Vac. Sci. Tech. B 1 (1983) 37.
11. F. H. M. Sanders, A. W. Kolfschoten, and J. Dieleman, J. Vac. Sci. Tech. A 2 (1984) 487.
12. D. J. Vitkavage, M. S. Ameen, and T. M. Mayer, J. Vac. Sci. Tech. A 2 (1984) 492.
13. T. J. Chuang, J. Chem. Phys. 76 (1982) 3828.

14. M. S. Slutsky and T. F. George, J. Chem. Phys. 70 (1979) 1231.

15. T. J. Chuang, J. Vac. Sci. Tech. 21 (1982) 798.

16. T. J. Chuang, J. Vac. Sci. Tech. 18 (1981) 638.

17. L. R. Danielson, M. J. Dresser, E. E. Donaldson, and D. R. Sandstrom, Surf. Sci. 71 (1978) 615.

18. P. S. Frederick and S. J. Hruska, Surf. Sci. 62 (1977) 707.

19. J. W. Coburn and H. F. Winters, J. Appl. Phys. 50 (1979) 3189.

20. H. F. Winters and J. W. Coburn, Appl. Phys. Lett. 34 (1979) 70.

21. T. J. Chuang, J. Appl. Phys. 51 (1980) 2614.

22. L. I. Civankiv, Sov. Phys. Solid State 17 (1974) 730.

23. V. T. Coon, Surf. Sci. 88 (1979) L42.

24. J. Harris, B. Kasemo, and E. Tornqvist, Chem. Phys. Lett. 52 (1977).

25. B. Kasemo, Phys. Rev. Lett. 20 (1974) 1114.

26. T. F. Gesell and E. T. Arakawa, Surf. Sci. 20 (1970) 174.

27. L. E. Brus and J. Comas, J. Chem. Phys. 54 (1971) 2771.

28. B. Kasemo, E. Tornqvist, and L. Wallden, Mater. Sci. Eng. 42 (1980) 23.

29. B. Kasemo and L. Wallden, Surf. Sci. (1975) 393.

30. B. Kasemo, E. Tornqvist, J. K. Norskov, and B. I.

Lundqvist, Surf. Sci. 89 (1979) 554.

31. T. P. Gesell and E. T. Arakawa, Surf. Sci. 33 (1972) 419.

32. J. Ferrante, ESLE Trans. 20 (1976) 328.

33. J. K. Norskov, D. M. Newns, and B. I. Lundqvist, Surf. Sci. 80 (1979) 179.

34. B. I. Lundqvist, O. Gunnarsson, H. Hjelmberg, and J. K. Norskov, Surf. Sci. 89 (1979) 196.

35. T. J. Chuang, Phys. Rev. Lett. 42 (1979) 815.

36. P. C. Zalm, L. J. Beckers, and F. H. M. Sanders, Nucl. Inst. Meth. 209 (1983) 561.

37. J. D. Chinn, I. Adesida, and E. D. Wolf, Appl. Phys. Lett. 43 (1983) 185.

38. C. I. H. Ashby and R. R. Rye, J. of Nucl. Mater. 103,104 (1981) 489.

39. C. I. H. Ashby and R. R. Rye, J. of Nucl. Mater. 92 (1980) 141.

40. C. I. H. Ashby, J. Vac. Sci. Tech. A 2 (1984) 639.

41. H. H. Madden, J. Vac. Sci. Tech. 13 (1976) 228.

42. V. I. Goldanskii, V. A. Namiot, and R. V. Khokhlov, Sov. Phys. JETP 43 (1976) 1226.

43. M. E. Umstead and M. C. Lin, J. Phys. Chem. 82 (1978) 2047.

44. S. Tachi, K. Miyake, and T. Tokuyama, Jap. J. Appl. Phys. 20 (1981) L411.

45. Y. Tu, T. J. Chuang, and H. F. Winters, J. Vac. Sci.

Tech. 18 (1981) 357.

46. W. Y. Lee, M. Chen, and J. M. Eldridge, J. Vac. Sci. Tech. 18 (1981) 359.

47. G. Smolinsky, E. A. Truesdale, D. N. K. Wang, and D. Maydan, J. Electrochem. Soc. 129 (1982) 1036.

48. B. A. Heath, J. Electrochem. Soc. 129 (1982) 396.

49. D. J. Sharp and J. K. G. Panitz, Surf. Sci. 118 (1982) 429.

50. Y. Margoninski, J. Appl. Phys. 47 (1976) 3868.

51. T. J. Chuang, J. Chem. Phys. 72 (1980) 6303.

52. R. G. Evans and P. C. Thonemann, Phys. Lett. 38A (1971) 398.

53. T. Kawai and T. Sakata, Chem. Phys. Lett. 69 (1980) 33.

54. D. R. Betteridge and J. T. Yardley, Chem. Phys. Lett. 62 (1979) 570.

55. M. A. Loudiana, A. Schmid, J. T. Dickinson, and E. J. Ashley, Surf. Sci. 141 (1984) 409.

56. F. A. Houle and T. J. Chuang, J. Vac. Sci. Tech. 20 (1982) 790.

57. M. J. Vasile, J. Appl. Phys. 51 (1980) 2510.

58. S. Matsuo, J. Vac. Sci. Tech. 17 (1980) 587.

59. P. Blank and K. Wittmaack, J. Appl. Phys. 50 (1979) 1519.

60. B. Navinsek, Prog. Surf. Sci. 7 (1975) 49.

61. P. Sigmund, Phys. Rev. 184 (1969) 383.

62. G. Carter and D. G. Armour, Thin Solid Films 80 (1981) 13.

63. J. Bohdansky and J. Roth, J. Appl. Phys. 51 (1980) 2861.

64. R. Behriseh (ed), Topics in Applied Physics 47 (1981).

65. A. Turos, W. F. van der Weg, D. Sigurd, and J. W. Mayer, J. Appl. Phys. 45 (1974) 2777.

66. R. Kelly, Surf. Sci. 100 (1980) 85.

67. R. Kelly and O. Auciello, Surf. Sci. 100 (1980) 135.

68. G. A. Samorjai, Principles of Surface Chemistry (Prentice-Hall Inc. 1972).

69. U. Von Gemmingen, Surf. Sci. 120 (1982) 334.

70. J. Ferron, E. V. Alonso, R. A. Baragiola, and A. Oliva-Florio, Surf. Sci. 120 (1982) 427.

71. D. Menzel, J. Vac. Sci. Tech. 20 (1982) 538.

72. P. R. Antoniewicz, Phys. Rev. B 21 (1980) 3811.

73. E. R. Moog, J. Unguris, and M. B. Webb, Surf. Sci. 134 (1983) 849.

74. P. Feulner, R. Treichler, and D. Menzel, Phys. Rev. B 24 (1981) 7427.

75. R. Franchy and D. Menzel, Phys. Rev. Lett. 43 (1979) 865.

76. D. Lichtman, Surf. Sci. 90 (1979) 579.

77. D. Lichtman, J. of Nucl. Mater. 53 (1974) 285.

78. W. P. Ellis, J. Vac. Sci. Tech. 14 (1977) 1316.

79. Y. Shapira and A. Friedenberg, Int. J. Mass Spec. Ion Phys. 36 (1980) 9.

80. C. L. Strecker, J. Appl. Phys. 52 (1981) 6921.

81. P. J. Feibelman and M. L. Knotek, Phys. Rev. B 18 (1978) 6531.

82. M. L. Knotek and P. J. Feibelman, Phys. Rev. Lett. 40 (1978) 964.

83. R. P. Holmstrom, J. Lagowski, and H. C. Gatos, Surf. Sci. 75 (1978) L781.

84. D. E. Ravaker, C. T. White, and J. S. Murday, Phys. Lett. 89A (1982) 211.

85. M. Salmeron and A. M. Baro, Surf. Sci. 29 (1972) 300.

86. B. Carriere and B. Lang, Surf. Sci. 64 (1977) 209.

87. T. R. Pian, N. Tolk, J. Kraus, M. M. Traum, J. Tully, and W. E. Collins, J. Vac. Sci. Tech. 20 (1982) 555.

88. J. F. O Hanlon, A Users Guide to Vacuum Technology (Wiley-Interscience 1980).

89. J. H. Holloway, Noble Gas Chemistry (Methuen and Co. Ltd. London 1968).

90. G. D. Sides and T. O. Tiernan, J. Chem. Phys. 65 (1976) 3392.

91. W. E. Falconer, M. J. Vasile, and F. A. Stevie, J. Chem. Phys. 66 (1977) 5335.

92. T. A. Flaim and P. D. Ownby, J. Vac. Sci. Tech. 8 (1971) 661.

93. K. L. Chopra, Thin Film Phenomena (1969).

94. A. W. Warner and C. D. Stockbridge, J. Appl. Phys. 34 (1963) 437.

95. E. Sollner, E. Beves, A. Biedermann, and D. Hammer, Vacuum 27 (1977) 367.

96. R. Niedermayer, N. Gladkick, and D. Hillecke, Ultra Micro Weight Determination in Controlled Environments (Interscience 1969) 217.

97. B. Ramadan, K. Piyakis, and J. F. Kos, Rev. Sci. Instr. 50 (1979) 867.

98. D. A. King, T. E. Madey, and J. T. Yates, Jr., J. Chem. Phys. 55 (1971) 3236.

99. D. A. King, T. E. Madey, and J. T. Yates, Jr., J. Chem. Soc. Far. Trans. 1 68 (1972) 1347.

100. C. D. Stockbridge, Ultra Micro Weight Determination in Controlled Environments (Interscience 1969) 147.

101. H. F. Winters, J. Vac. Sci. Tech. B 1 (1983) 927.

102. R. J. McIntyre and F. K. McTaggart, Austr. J. of Chem. 24 (1971) 2683.

103. P. Meakin, Phys. Rev. A 27 (1983) 2616.

104. H. J. Leamy, G. H. Gilmer, and A. G. Dirks, Current Topics in Material Science 6 (1980) 309.

105. R. L. Lusk, SPIE Thin Film Tech. Spec. Appl. 346 (1982) 48.

106. L. H. Bennett (ed.), Electronic Density of States, NBS Special Publication 323 (1971) 53.

107. F. C. Brown, The Physics of Solids, W. A. Benjamin

Inc. (1967).

108. J. D. Patterson, Introduction to the Theory of Solid State Physics, Addison-Wesley (1971).

109. R. C. Weast, CRC Handbook of Physics and Chemistry 57th ed., CRC Press (1977) E-82.

110. G. R. Floyd and R. H. Prince, Surf. Sci. 59 (1976) 631.

111. C. Park, M. Kramer, and E. Bauer, Surf. Sci. 109 (1981) L533.

112. M. A. Loudiana, J. T. Dickinson, and E. J. Ashley, J. Vac. Sci. Technol. A3 (1985) 647.

DISTRIBUTION LIST

Dr. James Stanford
Physical Optics Branch
Code 3818
Naval Weapons Center
China Lake, CA 93555

Dr. Bobby Junker
Head, Physics Division
Code 1112
Office of Naval Research
800 North Quincy St.
Arlington, VA 22217

Dr. Robert Behringer
Office of Naval Research
Western Regional Office
1030 East Green Street
Pasadena, CA 91106

James R. Delaney
ONR Representative
University District Bldg., Rm. 42
1107 NE 45th Street
Seattle, WA 98195

E. J. Friebele
Code 6570
Naval Research Laboratory
Washington, D. C. 20375

Director
Naval Research Laboratory
Code 2627
Washington, D. C. 20375
(6 copies)

Defense Technical Information Center
Bldg. 5, Cameron Station
Alexandria, Virginia 22314
(12 copies)